SUPPORTING INFORMATION

A bimetallic carbide derived from MOF precursor for increasing electrocatalytic oxygen evolution activity**

Jinjie Qian,*[a] Ting-Ting Li,[b] Yue Hu[a] and Shaoming Huang*[a]

[a]*College of Chemistry and Materials Engineering, Wenzhou University, Wenzhou 325035, P. R. China.*

[b] *Research Center of Applied Solid State Chemistry, Ningbo University, Ningbo, 315211, P. R. China*

**To whom correspondence should be addressed: E-mail: jinjieqian@wzu.edu.cn; smhuang@wzu.edu.cn; Tel: 86-577-88373064.*

Table of Content

S1. Materials and Methods

1.1. Materials and Instruments.

Reactions were carried out in 35 ml pressure-resistant tubes under autogenous pressure. All the reactants are of reagent-grade quality and used as commercially purchased without further purification.

In the LSV test, the IrO_2@CC reference electrode was also examined at the basic conditions for electrochemical comparison, where the IrO_2 sample is also purchased from commercial supplier.

The power X-ray diffraction patterns (PXRD) were collected by a Bruker D8 Advance using Cu Kα radiation (λ = 0.154 nm).

Single gas adsorption measurements were performed in the Accelerated Surface Area and Porosimetry 2020 (ASAP2020, where the bulk **InOF-16** materials were determined in a clean ultra high vacuum system and the N_2 sorption measurement was performed at 77 K.

Thermogravimetric analyses were recorded on a NETZSCH STA 449C unit at a heating rate of 10 $^{o}C\cdot min^{-1}$ under flowing nitrogen atmosphere.

Scanning transmission electron microscopy (STEM) and energy dispersive X-ray spectroscopy (EDS) analyses were carried out under JEOL JEM-2100F microscope operating at an accelerating voltage of 200 kV.

1.2. Synthesis of $[Me_2NH_2]_2[In_3(BTC)_5][Co_2(DMF)_6]$•Guest (InOF-16 = BMM-8).

A mixture of $InCl_3\cdot 4H_2O$ (30 mg), $Co(NO_3)_3\cdot 6H_2O$ (30 mg) and H_3BTC (20 mg) in *N,N'*-dimethylformamide (DMF) (5 mL) with an additional 0.05 ml HNO_3 (65 wt %) was placed in a 35 mL pressure-resistant tube, which was inserted into an oven holding at 85 ^{o}C for 1 week, and then gradually cooled to room-temperature. After centrifugated and washed by fresh ethanol, the light pink triangle-prism-shaped of **InOF-16** single crystals were obtained in *ca*. 50% yield based on the organic ligand. Elemental analysis was calculated for **InOF-16**: C, 35.85%; H, 4.36%; N, 4.99%.

Found: C, 35.94/35.82%; H, 4.41/4.45%; N, 4.98/4.87%.The phase purity of the sample was confirmed by powder X-ray diffraction (Figure S5).

1.3. Synthesis of $[Me_2NH_2][Co_3(\mu_3\text{-}OH)(BTC)_2(H_2O)]$•Guest (FJI-6).

A mixture of $Co(ClO_4)_2 \cdot 6H_2O$ (0.15 mmol, 57 mg), H_3BTC (0.10 mmol, 20 mg) in 5.0 ml N,N'-Dimethylacetamide (DMA) with an additional HBF_4 (0.4 ml, Tetrafluoroboric acid, 40% in water) was sealed in a 25 ml glass vial, which was heated at 100 ^oC for 5 days, and cooled down to room temperature. After washed by fresh DMA, the red crystals of **FJI-6** were obtained in ca. 50% yield based on the H_3BTC ligand. Elemental analysis was calculated for **FJI-6**: C, 34.41%; H, 3.04%; N, 2.01%. Found: C, 33.31%; H, 2.94%; N, 1.94%. ICP data: Zn, 10.19% and Co, 9.38%. The phase purity of the sample is confirmed by PXRD (Figure S6).

1.4. Synthesis of $[Me_2NH_2]_3[In_3(BTB)_4]$•Guest (InOF-9).

A mixture of $In(NO_3)_3$ (0.10 mmol, 33 mg) and H_3BTB (0.10 mmol, 44 mg, H_3BTB = 1,3,5-tris(4-carboxyphenyl)benzene) in the mixing solvent of DMF and DMA was sealed in a 25 ml autoclave, which was heated at 120 ^oC for four days, and cooled gradually to room temperature in another day. After washed by fresh acetonitrile, the light yellow crystals were obtained in *ca*. ~50% yield based on the H_3BTB ligand. Elemental analysis was calculated for **InOF-9**: C, C, 50.22%; H, 6.06%; N, 3.20%.. Found: C, 49.77%; H, 5.52%; N, 2.99%. The phase purity of the sample is also confirmed by PXRD (Figure S6).

1.5. Synthesis of In_2O_3, Co_3O_4, InOF-16-Ar/O_2-T materials Hybrids.

Pristine **FJI-6 InOF-9**, **InOF-16** was synthesized according to the above-mentioned method. All annealing processes were conducted at a heating rate of 5 °C min^{-1} under a stream of O_2/Ar (0.5 sccm) after excluding air by flushing Ar for 30 min (Note: sccm denotes standard cubic centimetres per minute]) The as-prepared microcrystals (200 mg) were weighed in a quartz boat and transferred into a quartz tube. The tube was sealed and placed inside a CVD furnace, where the carbonization

was performed at 550, 700 and 1000 °C under the continuous flowing for 3 hours. After gradually cooling down to room temperature, the titled black powders **In_2O_3, Co_3O_4, InOF-16-Ar/O_2-T** were successfully obtained. The phase purity of the corresponding samples were also confirmed by powder X-ray diffraction. (Figure S7-9)

Scheme 1. Synthesis of InOF-16 and InOF-16-Ar/O_2-T materials at the different high temperatures in oxygen or argon atmosphere

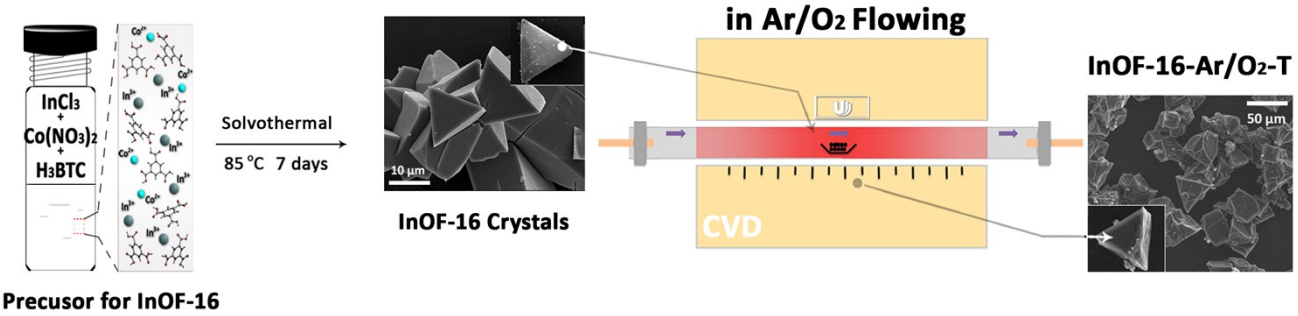

1.6. Single-Crystal X-ray Crystallography. The structure data of **InOF-16** was collected on a SuperNova, Dual, Cu at zero, Atlas diffractometer. The crystal was kept at 99.99(16) K during data collection. By using Olex2,[S1] the structure was solved with the ShelXS[S2] structure solution program using Direct Methods and refined with the ShelXL[S3] refinement package using Least Squares minimisation. Crystallographic data and structure refinement parameters for this crystal is summarized in Table S1. We employed PLATON/SQUEEZE to calculate the contribution to the diffraction from the solvent region and thereby produced a set of solvent-free diffraction intensities. The coordinated H_2O and DMF in this structure are determined according to charge balance and a rational experimental bond and angle parameters which is well consistent with the experiment data ever reported.

When removing the isolated and/or disordered guest molecules, the main framework is defined as a negative $[In_3(BTC)_5][Co_2(DMF)_6]^{2-}$ network where we assume *in-situ* formed charge-balancing disordered $Me_2NH_2^+$ cations residing within the void, which is the *in-situ* formed by-products of the DMF solvent molecules during the solvothermal reaction.[S4] The final formula was calculated from the

SQUEEZE results combined with elemental analysis data and TGA data. More details on the crystallographic studies as well as atomic displacement parameters are given in Supporting Information as CIF files. Crystallographic data for the structure reported in this paper has been deposited. The following crystal structure has been deposited at the Cambridge Crystallographic Data Centre and allocated the deposition number (CCDC No.) 1527119 for **InOF-16**. These data can be obtained free of charge via *www.ccdc.cam.ac.uk/data_request/ cif.*

Table S1. Summary of Crystal Data and Refinement Results for InOF-16

Items	**InOF-16**
formula	$C_{6.25}HCo_{0.17}In_{0.25}NO_3$
Mass	176.61
crystal system	Hexagonal
space group	*P*-62m (#. 189)
a (Å)	18.2416(13)
b (Å)	18.2416(13)
c (Å)	9.9938(7)
α (°)	90.00
β (°)	90.00
γ (°)	120.00
V (Å^3)	2880.0(4)
T (K)	173 (2)
Z	12
F(000)	1035
R_{int}	0.0624
R_1 (I>2σ(I))	0.1748
wR_2 (all reflections)	0.1757

S2. Additional Structure Images

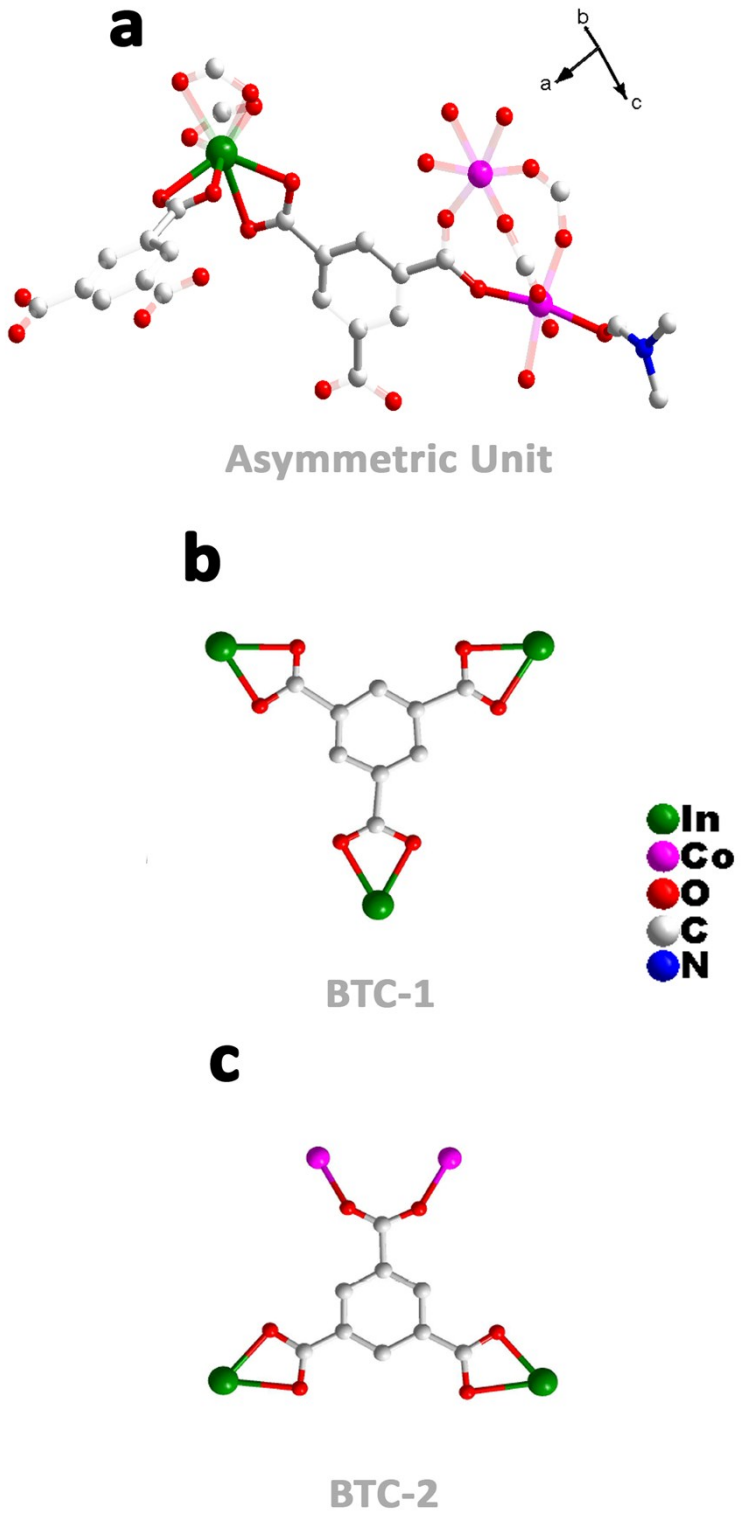

Figure S1. (a) The asymmetric unit of bimetallic single crystal structure for **InOF-16**. (b)~(c) two types of BTC ligands in this structure.

S3. Topological Analysis

Topology for **BTC-1**

Ligand BTC-1 links by bridge ligands and has

Common vertex with					R(A-A)	
[In(COO)$_4$]	1.0000	0.5931	0.0000	(1 1 0)	5.533A	1
[In(COO)$_4$]	0.4069	0.4069	0.0000	(0 0 0)	5.533A	1
[In(COO)$_4$]	0.5931	0.0000	0.0000	(1 0 0)	5.533A	1

Topology for **BTC-2**

Ligand BTC-2 links by bridge ligands and has

Common vertex with					R(A-A)	
Co$_2$(COO)$_3$	0.0000	0.0000	0.5000	(0 0 0)	5.084A	1
[In(COO)$_4$]	0.4069	0.4069	1.0000	(0 0 1)	5.517A	1
[In(COO)$_4$]	0.4069	0.4069	0.0000	(0 0 0)	5.517A	1

Topology for SBU **[In(COO)$_4$]**

SBU [In(COO)$_4$] links by bridge ligands and has

Common vertex with					R(A-A)	
BTC-2	0.2787	0.2787	-0.5000	(0 0-1)	5.517A	1
BTC-2	0.2787	0.2787	0.5000	(0 0 0)	5.517A	1
BTC-1	0.3333	0.6667	0.0000	(0 1 0)	5.533A	1
BTC-1	0.6667	0.3333	0.0000	(0 0 0)	5.533A	1

Topology for **Cobalt paddle-wheel**

SBU dimer Cobalt paddle-wheel links by bridge ligands and has

Common vertex with					R(A-A)	
BTC-2	0.2787	0.2787	0.5000	(0 0 0)	5.084A	1
BTC-2	0.0000	-0.2787	0.5000	(0 0 0)	5.084A	1
BTC-2	-0.2787	0.0000	0.5000	(0 0 0)	5.084A	1

Structural group analysis

Structural group No 1

Structure consists of 3D framework

Coordination sequences

BTC-1: 1 2 3 4 5 6 7 8 9 10

Num 3 9 18 38 48 83 93 152 153 233

Cum 4 13 31 69 117 200 293 445 598 831

BTC-2: 1 2 3 4 5 6 7 8 9 10

Num 3 8 16 34 43 82 91 146 151 232

Cum 4 12 28 62 105 187 278 424 575 807

[In(COO)$_4$]: 1 2 3 4 5 6 7 8 9 10

Num 4 8 22 30 56 68 114 122 190 188

Cum 5 13 35 65 121 189 303 425 615 803

[Co$_2$(COO)$_3$]: 1 2 3 4 5 6 7 8 9 10

Num 3 6 18 26 57 68 117 122 189 188

Cum 4 10 28 54 111 179 296 418 607 795

TD10=809

Vertex symbols for selected sublattice

BTC-1 Point (Schlafli) symbol:{8^3}

Extended point symbol:[8(4).8(4).8(4)]

BTC-2 Point (Schlafli) symbol:{8^3}

Extended point symbol:[8(4).8(4).8(4)]

[In(COO)$_4$] Point (Schlafli) symbol:{8^6}

Extended point symbol:[8(2).8(2).8(3).8(3).8(3).8(3)]

[Co$_2$(COO)$_3$] Point (Schlafli) symbol:{8^3}

Extended point symbol:[8(4).8(4).8(4)]

Point (Schlafli) symbol for net: {8^3}2{8^6}

3,3,3,4-c net with stoichiometry (3-c)2(3-c)3(3-c)(4-c)3; 4-nodal net

Topological type: **mco** (topos&RCSR.ttd) {8^3}2{8^6} - VS [8(4).8(4).8(4)] [8(4).8(4).8(4)] [8(4).8(4).8(4)] [8(2).8(2).8(3).8(3).8(3).8(3)] (71251 types in 10 databases)

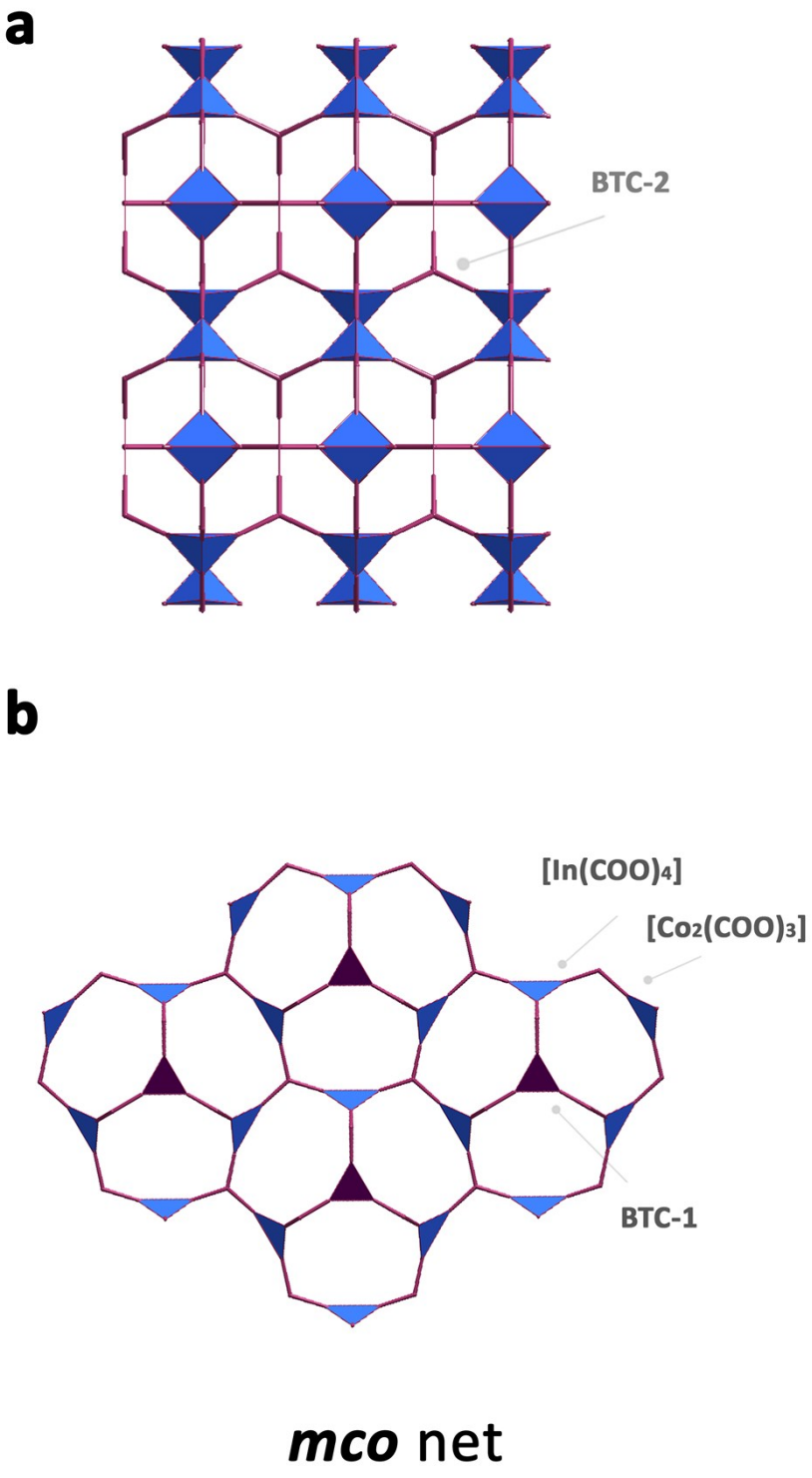

Figure S2. Topological representation and analysis for **InOF-16** Structure.

S4. N_2 isotherms

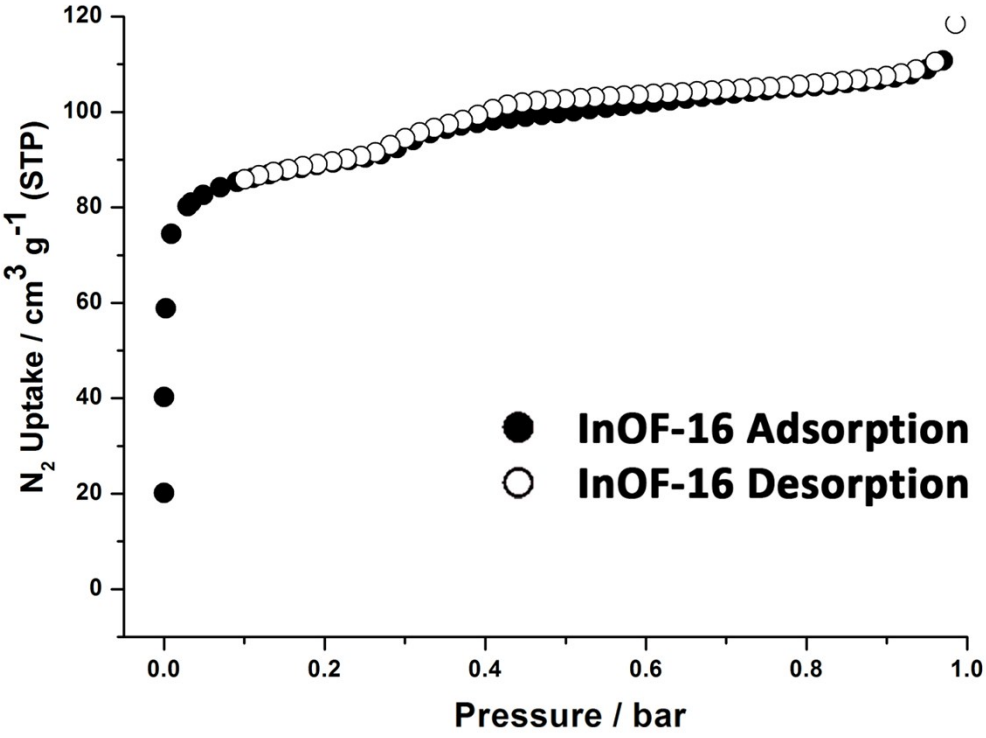

Figure S3a The experimental N_2 adsorption/desorption isotherms at 77 K for activated **InOF-16** samples.

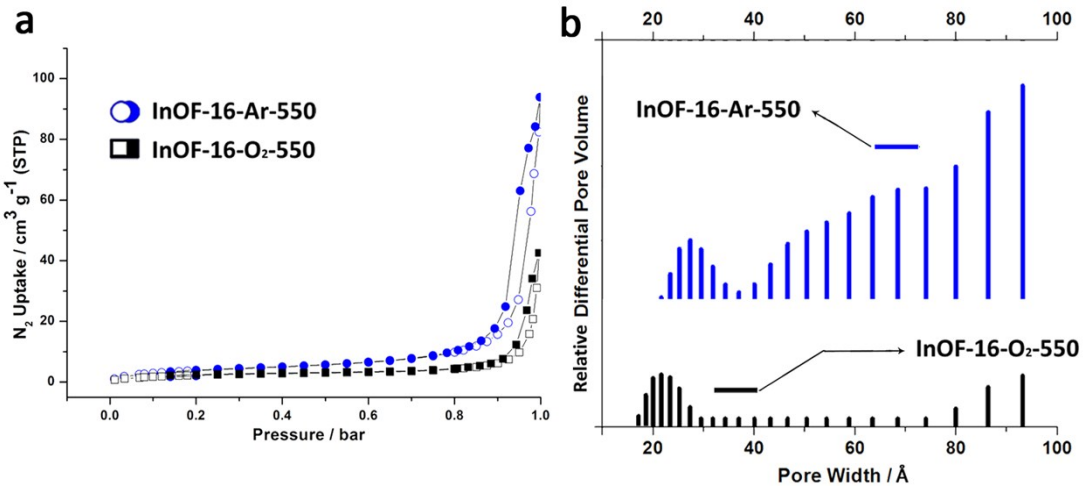

Figure S3b. (a) N_2 adsorption-desorption isotherms at 77 K for the obtained composites; (b) Pore size distribution analysis for pyrolyzed products.

The N_2 adsorption-desorption isotherms at 77 K have been further performed to evaluate the specific surface area and the porosity of the prepared oxides and carbides composite. As shown in Figure 3b, the isotherm shows type IV hysteresis loop at relative pressure 0.7 ~ 1.0 further indicating its mesoporous structure after the calcination process.

Meanwhile, we learn that there is of very low N_2 capacity less than 0.1 bar, between 0.1 and 0.8, which means the gas adsorption capacity in microsized pore and external surface is weak. And the **InOF-16-Ar-550** material surpasses **InOF-16-O_2-550** a little might due to the preserved carbon matrix, which is supported by pore size distribution (PSD) analyses by using DFT method, which exhibits a more mesoporous distribution for **InOF-16-Ar-550** than that of product in oxygen flowing.

S5. TGA Data

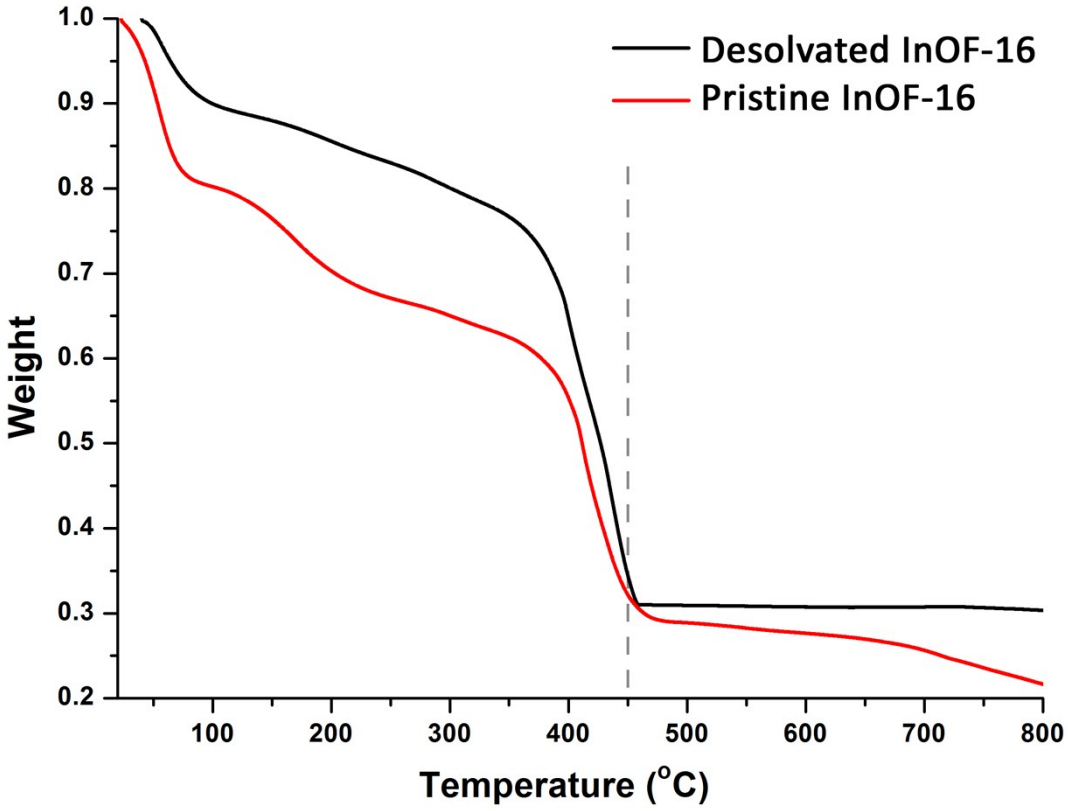

Figure S4. TGA curves for pristine and desolvated **InOF-16** samples before and after activation process.

S6. PXRD Patterns

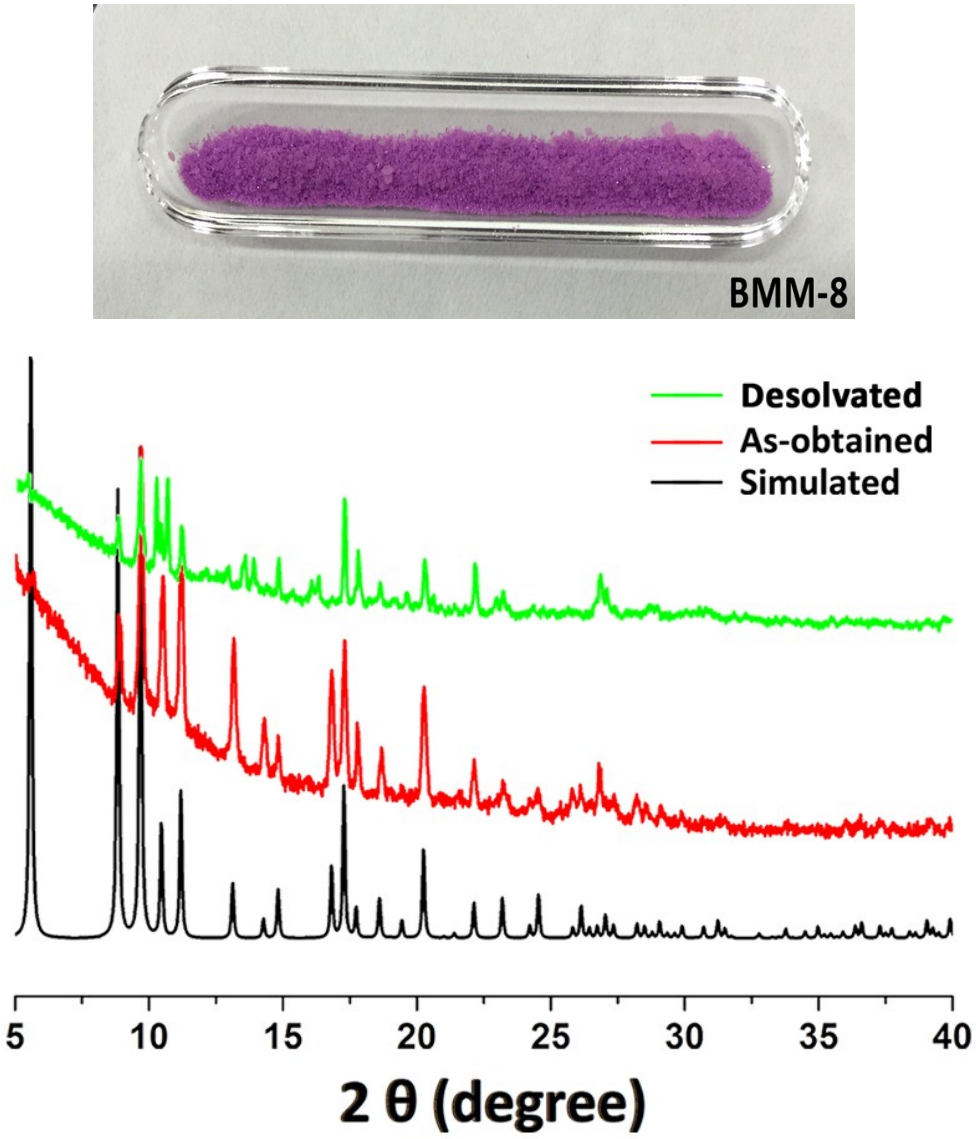

Figure S5. PXRD patterns of **InOF-16**: simulated from the crystallographic information file (black); from the as-prepared sample (red); from the desolvated sample (green).

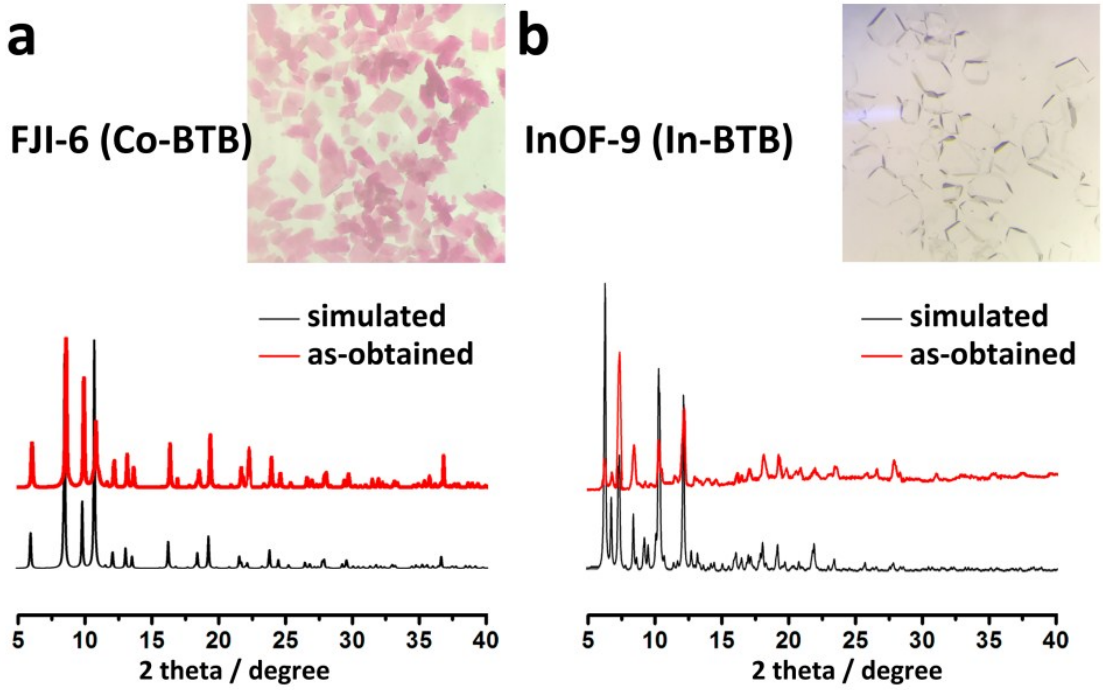

Figure S6. The PXRD patterns of as-prepared Co-MOF (Right) and In-MOF (Left). The insets show the photographs of both crystals under lab microscopy.

We have prepared pure monometallic Co-MOF (**FJI-6**: $[Me_2NH_2][Co_3(\mu_3\text{-}OH)(BTC)_2(H_2O)]\cdot$Guest) and In-MOF (**InOF-9**: $[Me_2NH_2]_3[In_3(BTB)_4]$), where Co-BTC is based on the same ligand H_3BTC (H_3BTC = 1,3,5-benzenetricarboxylic acid) we used for our **BMM-8** with similar porosity, while In-MOF is constructed by the elongated ligand H_3BTB (H_3BTB = 1,3,5-tris(4-carboxyphenyl)benzene), which exhibits microporous material characteristics with the saturated nitrogen uptake of 297.1 $cm^3\ g^{-1}$ at 77 K, corresponding to BET and Langmuir surface area of 1121.9 $m^2\ g^{-1}$ and 1287.6 $m^2\ g^{-1}$, respectively. Both materials have been successfully prepared according to our previous literatures, and then pyrolyzed in the oxygen atmosphere to obtain the pure Co_3O_4 and In_2O_3 from **FJI-6** and **InOF-9**, respectively (Figure S6).

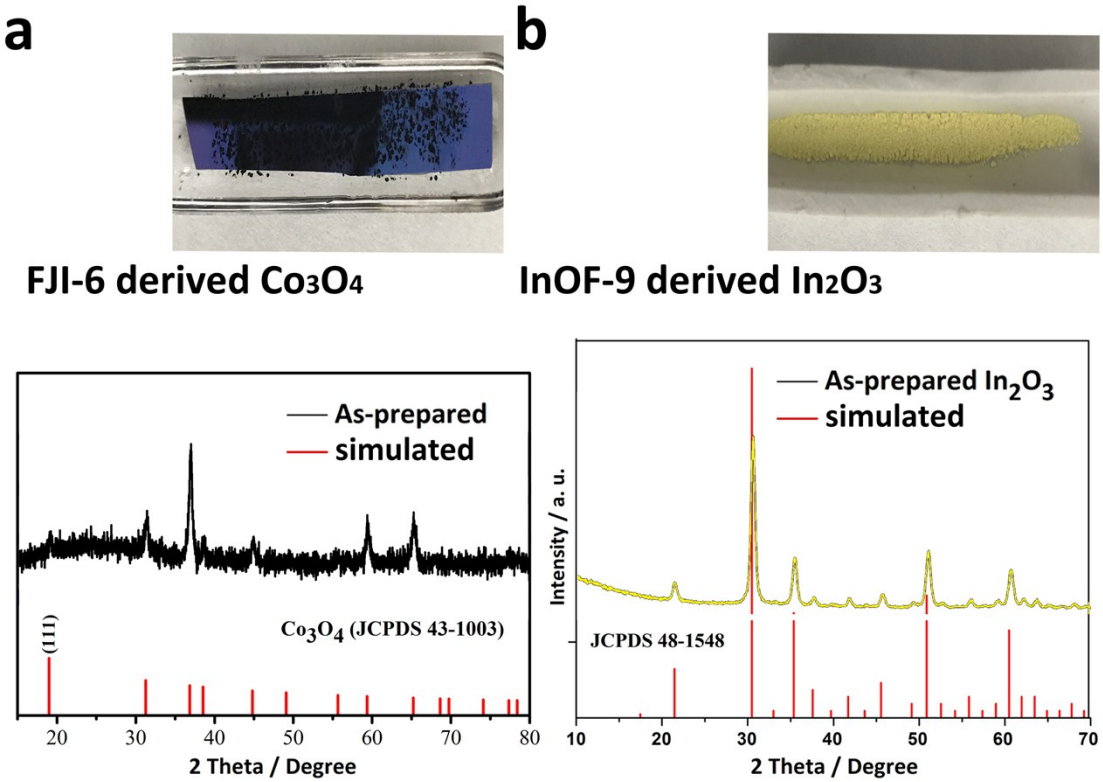

Figure S7. The PXRD patterns of as-prepared Co-MOF-derived Co_3O_4 (Right) and In-MOF-derived In_2O_3 (Left). The insets show the photographs of both materials after the pyrolyzed process in the combustion boat.

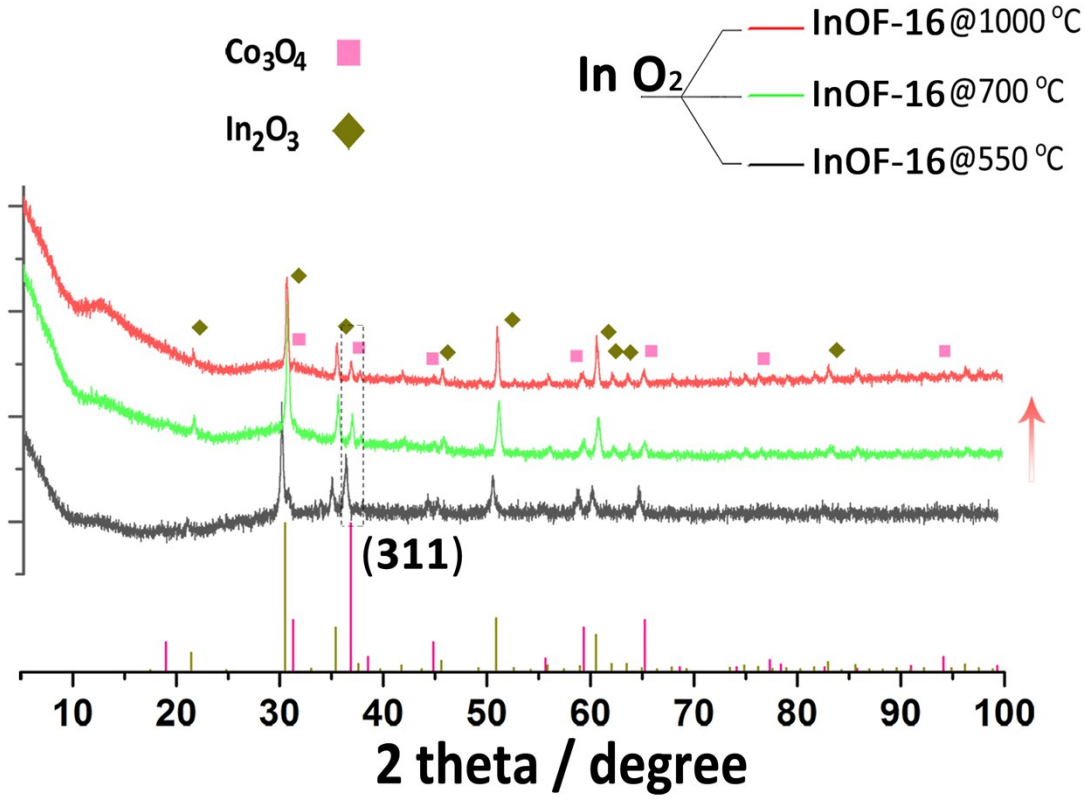

Figure S8. PXRD patterns of **InOF-16-O_2-550/700/1000** materials: simulated from the crystallographic information file (gold line = In_2O_3; pink line = Co_3O_4); from the as-prepared sample at different temperatures (black pattern at 550 °C; green pattern at 700 °C; red pattern at 1000 °C).

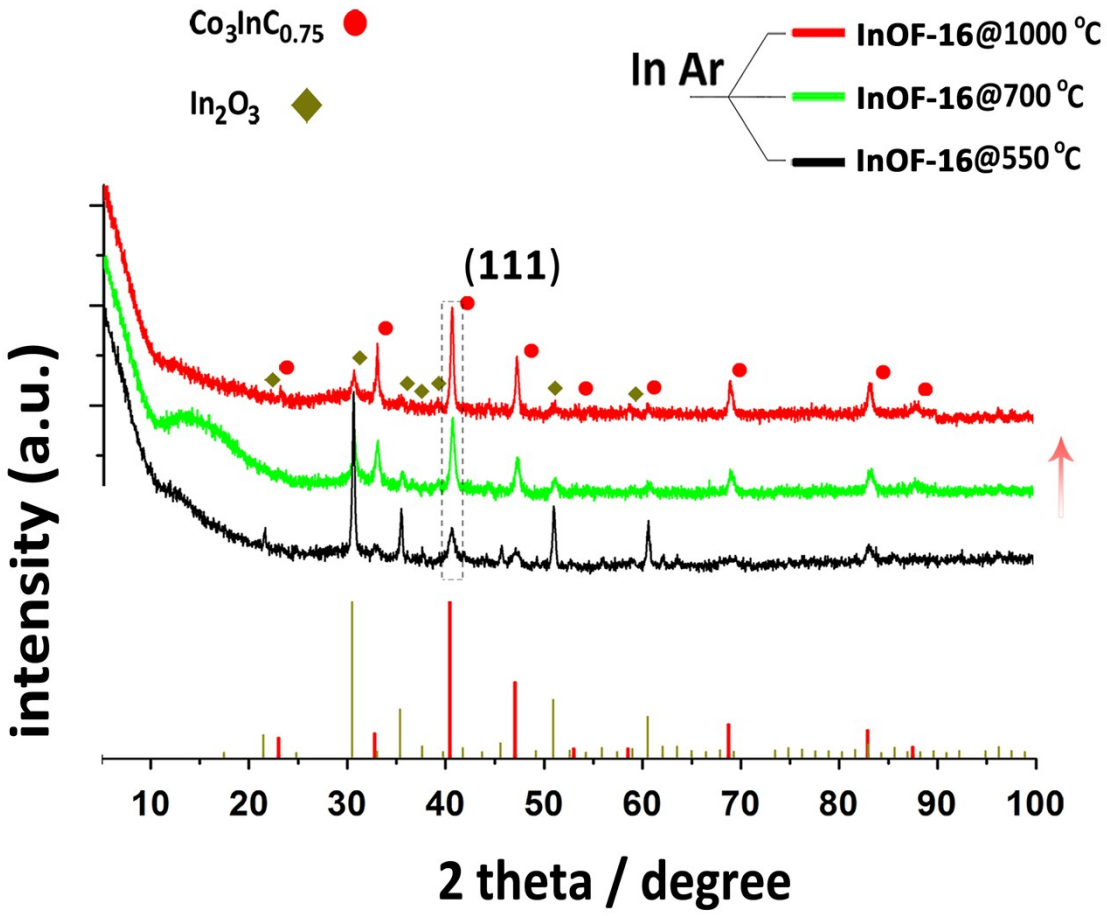

Figure S9. PXRD patterns of **InOF-16-Ar-550/700/1000** materials: simulated from the crystallographic information file (gold line = In_2O_3; red line = $Co_3InC_{0.75}$); from the as-prepared sample at different temperatures (black pattern at 550 °C; green pattern at 700 °C; red pattern at 1000 °C).

Generally speaking, we have done the PXRD test to confirm the composition of our products (two kinds of oxides in **InOF-16-O_2-550** [In_2O_3 and Co_3O_4], and oxide and carbide in **InOF-16-Ar-550** [In_2O_3 and $Co_3InC_{0.75}$]), as depicted in Figure S8, S9. Then we conduct the X-ray photoelectron spectroscopy and energy dispersive spectroscopy, which show both samples consist of indium, cobalt and carbon elements and their valent state. Below is the structure of $Co_3InC_{0.75}$.

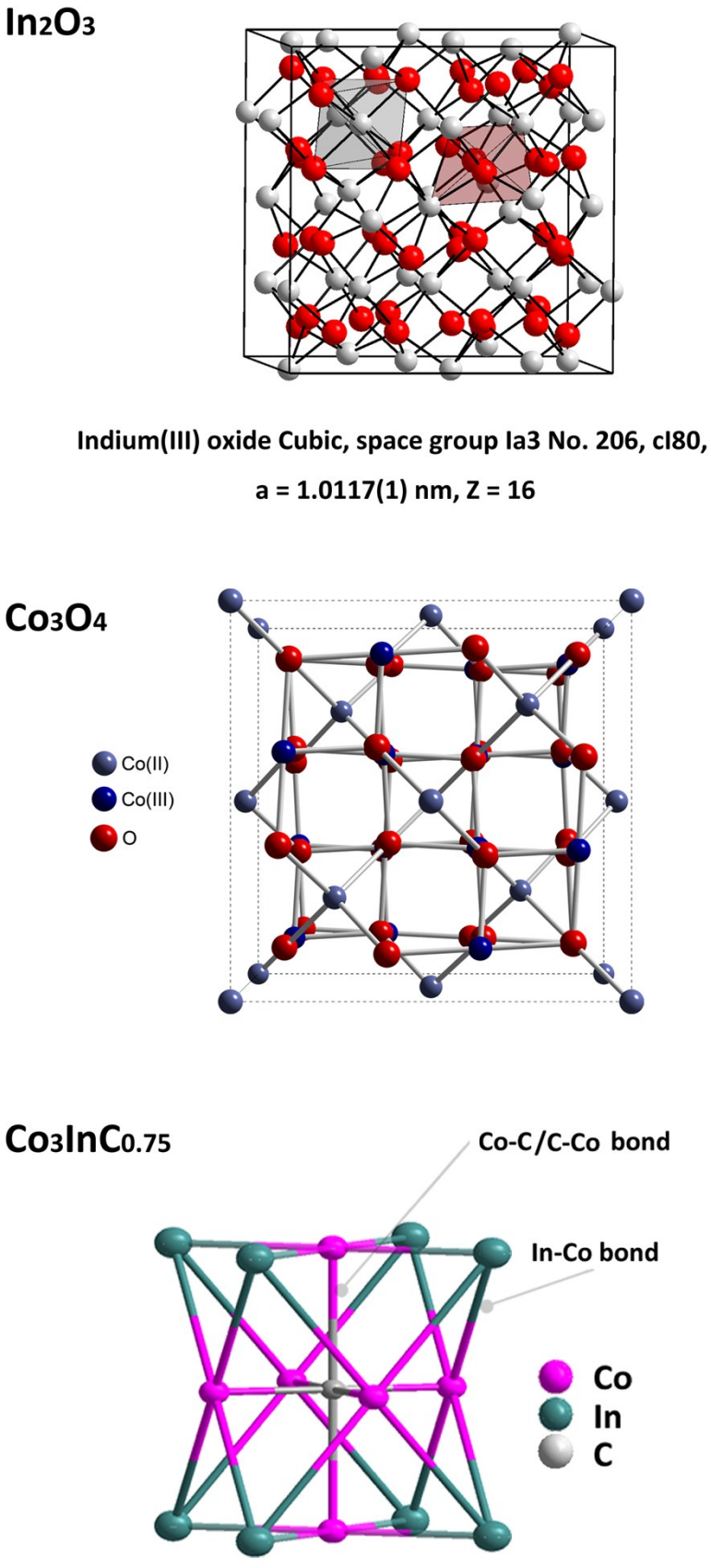

Figure S10. The structure of indium oxide, Co(II,III) oxide and carbide $Co_3InC_{0.75}$.

S7. SEM for InOF-16-O_2/Ar-1000 Materials

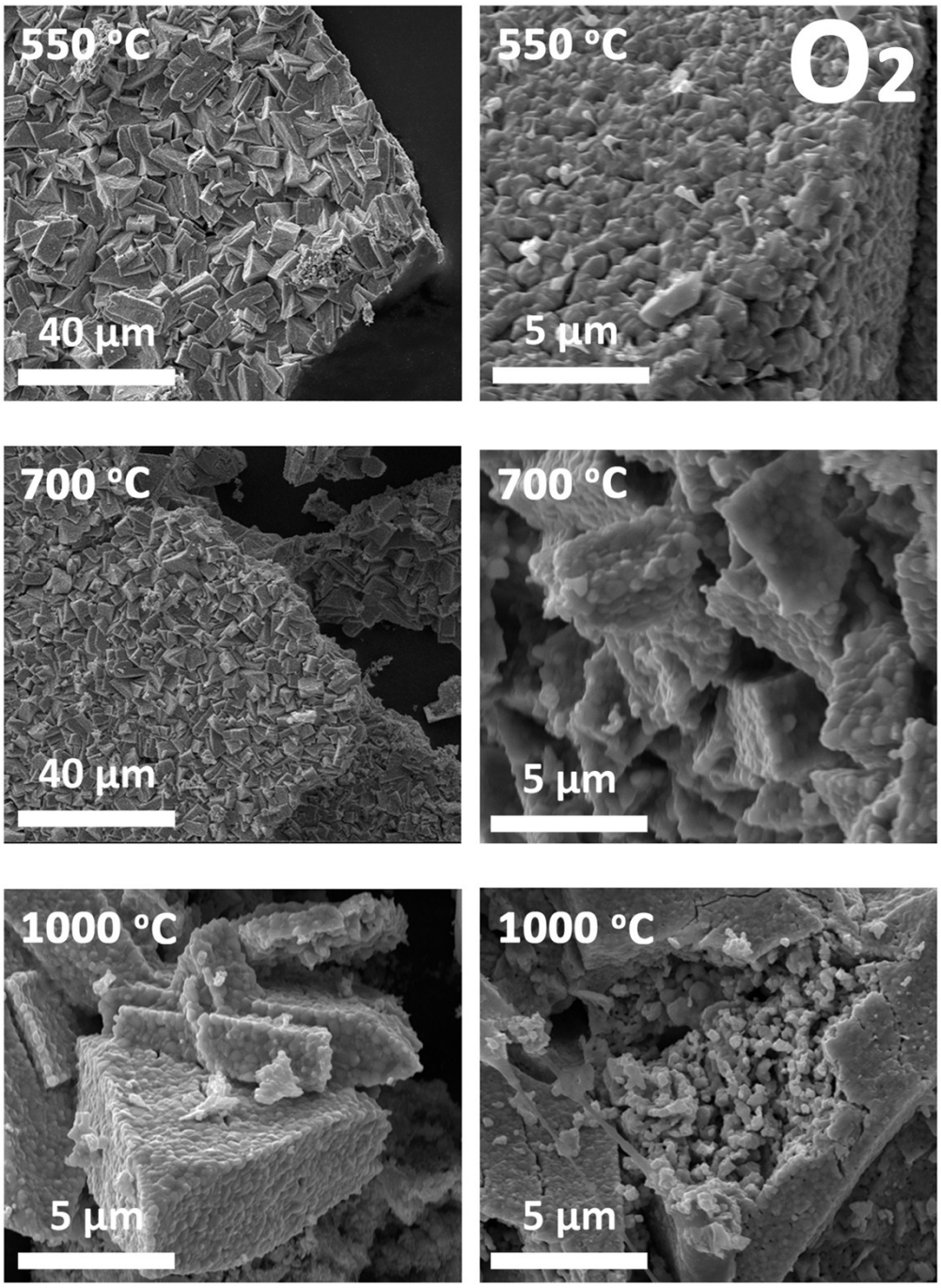

Figure S11. SEM images of **InOF-16-O_2-550/700/1000** samples.

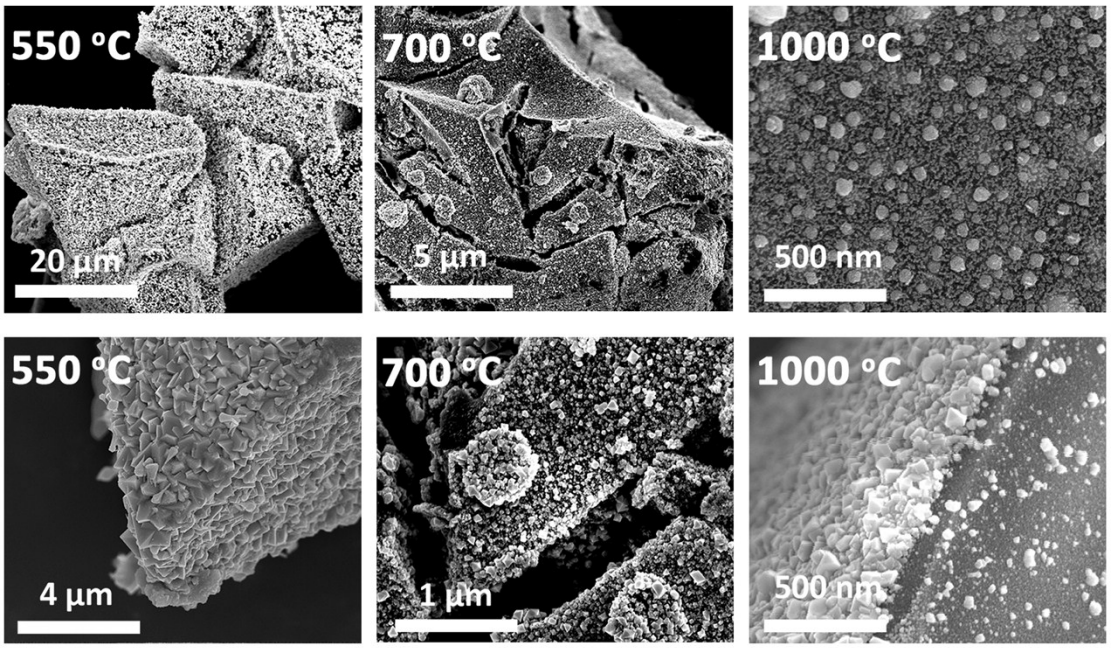

Figure S12. SEM images of **InOF-16-Ar-550/700/1000** samples.

In particular, what we should mention here is that though the retention of the MOF morphology after both thermal treatment, the final product looks like having the rough surface with smooth nanoparticles constituting the external layer pyrolyzed in the oxygen (Figure S11)., while the product have a surface with sharp single-crystal-like NPs of inorganic components in the argon flowing (Figure S12).

S8. TEM and HR-TEM for InOF-16-O_2/Ar-1000 Materials

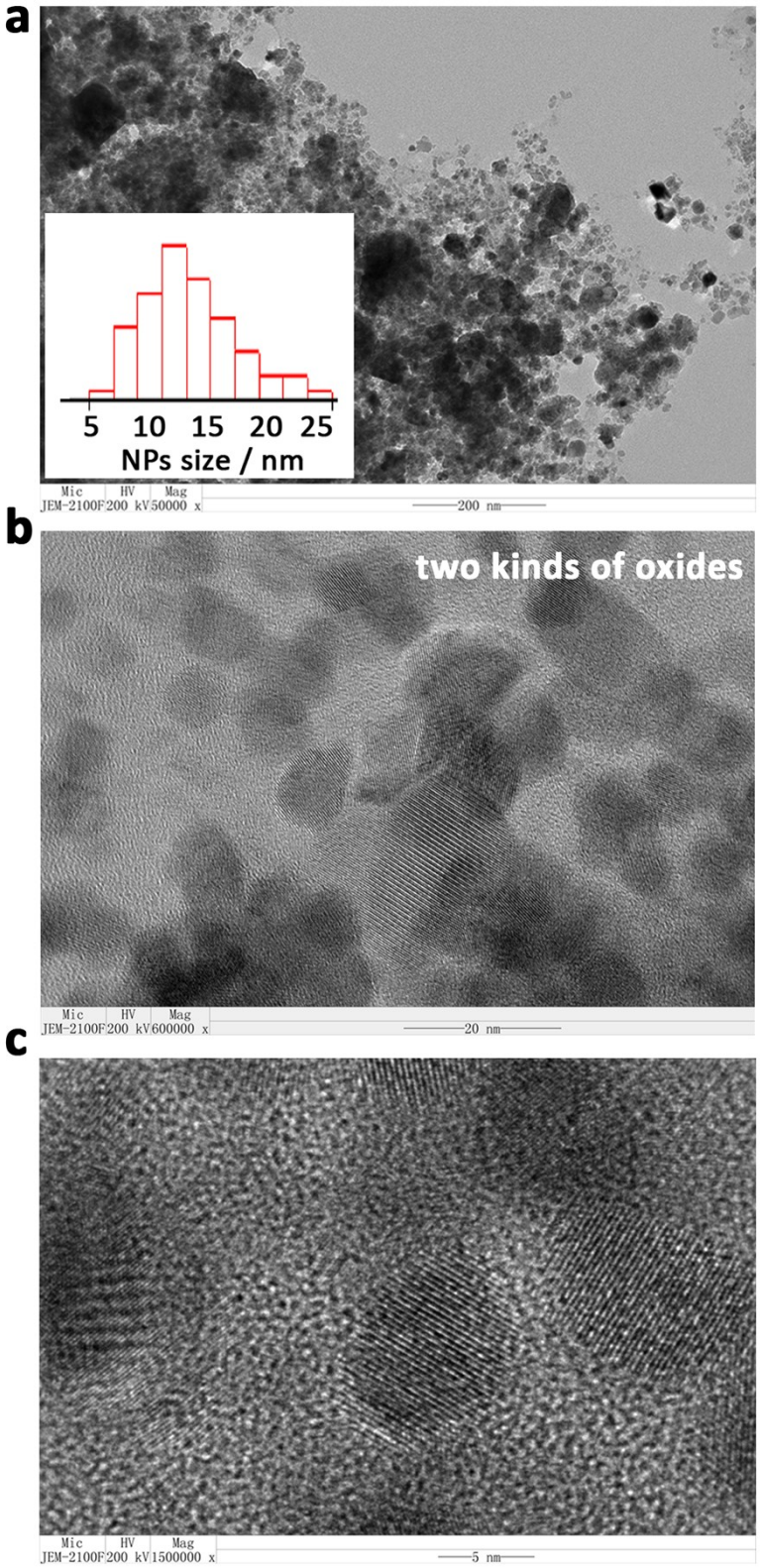

Figure S13. Structural characterization: TEM and HR-TEM images of calcinated **InOF-16-O_2-550/700/1000** materials, indicating a binary oxides coexisting structure.

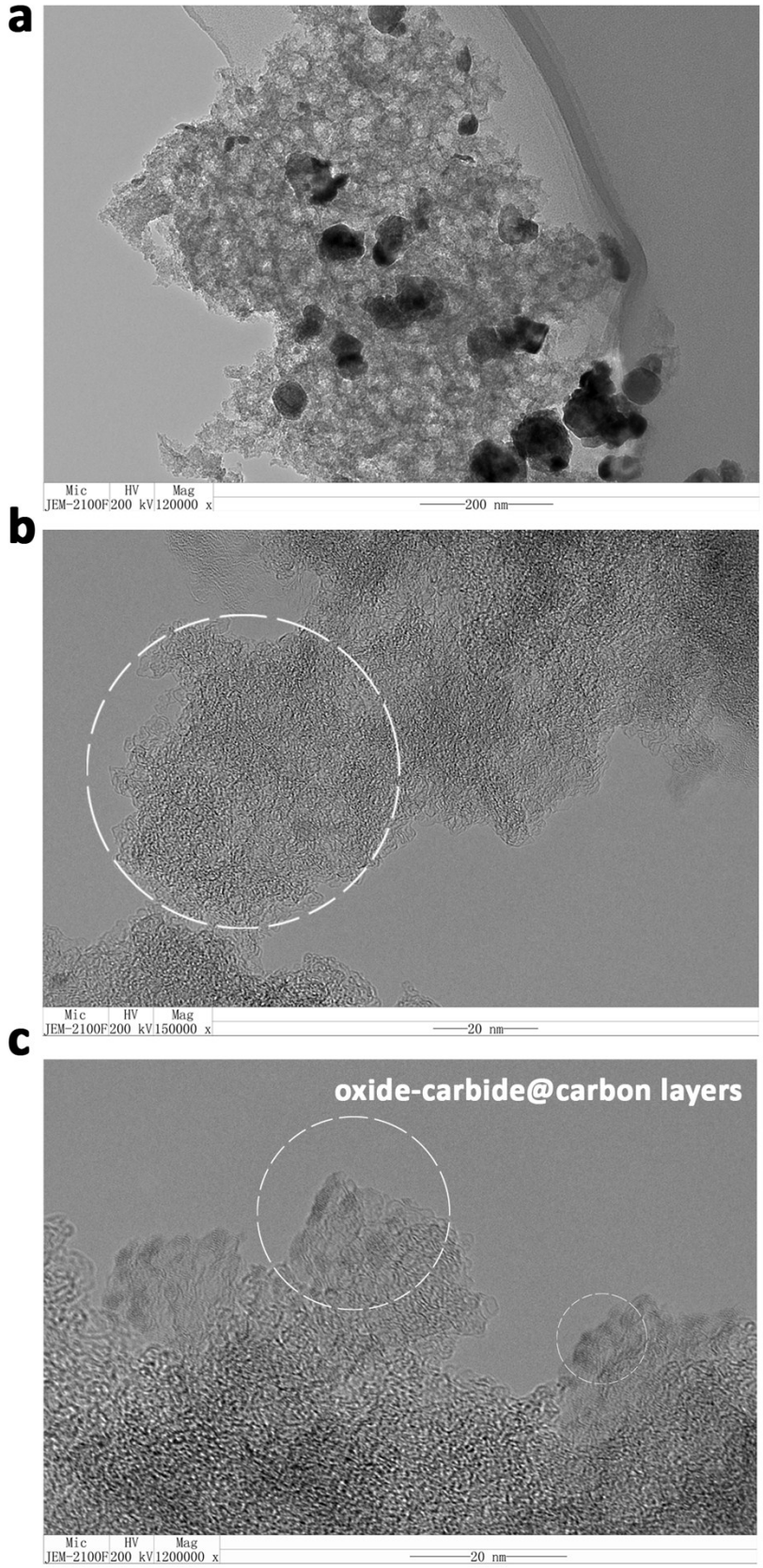

Figure S14. Structural characterization: TEM and HR-TEM images of calcinated **InOF-16-Ar-550/700/1000** materials, indicating a oxide-carbide@carbon structure.

S9. ICP and EDX analysis of pyrolyzed materials

In order to investigate the percentage of composite under different temperature, we have conducted the inductively coupled plasma (ICP) and EDS tests. Prior to the ICP test, the **InOF-16-O_2-550/700/1000** samples are desovled in the acidic solution. We can learn that with the temperature, the percentage of indium increases, while the cobalt percentage indeed decreases from 15.5% (550 ^oC) to 7.5% (1000 ^oC).

Table S2. EDS data: the weight percentage of InOF-16-O_2-T

Items (EDS element)	Percentage (In/Co)	
InOF-16-O_2-550	40.1%	15.5%
InOF-16-O_2-700	44.1%	14.9%
InOF-16-O_2-1000	55.8%	7.5%

Table S3. ICP data: the weight ratios of In/Co in InOF-16-O_2-T

Items (ICP)	Weight ratios of In/Co
InOF-16-O_2-550	2.94
InOF-16-O_2-700	3.02
InOF-16-O_2-1000	4.53

Meanwhile, we have also collected the ICP and EDS tests to probe into the percentage of composite under different temperature for **InOF-16-Ar-550/700/1000** samples. Similarly, it reveals that the percentage of indium increases, while the cobalt percentage indium from 12.5% (550 ^{o}C) to 40.3% (1000 ^{o}C) with the increasing temperature.

Table S3. EDS data: the weight percentage of InOF-16-Ar-550/700/1000

Items (EDS element)	Percentage (In/Co)	
InOF-16-Ar-550	57.5%	12.5%
InOF-16-Ar-700	42.5%	32.5%
InOF-16-Ar-1000	39.6%	40.3%

Table S4. ICP data: the weight ratios of In/Co in InOF-16-Ar-550/700/1000

Items (ICP)	Weight ratios of In/Co
InOF-16-Ar-550	2.31
InOF-16-Ar-700	0.69
InOF-16-Ar-1000	0.55

S10. Raman spectra

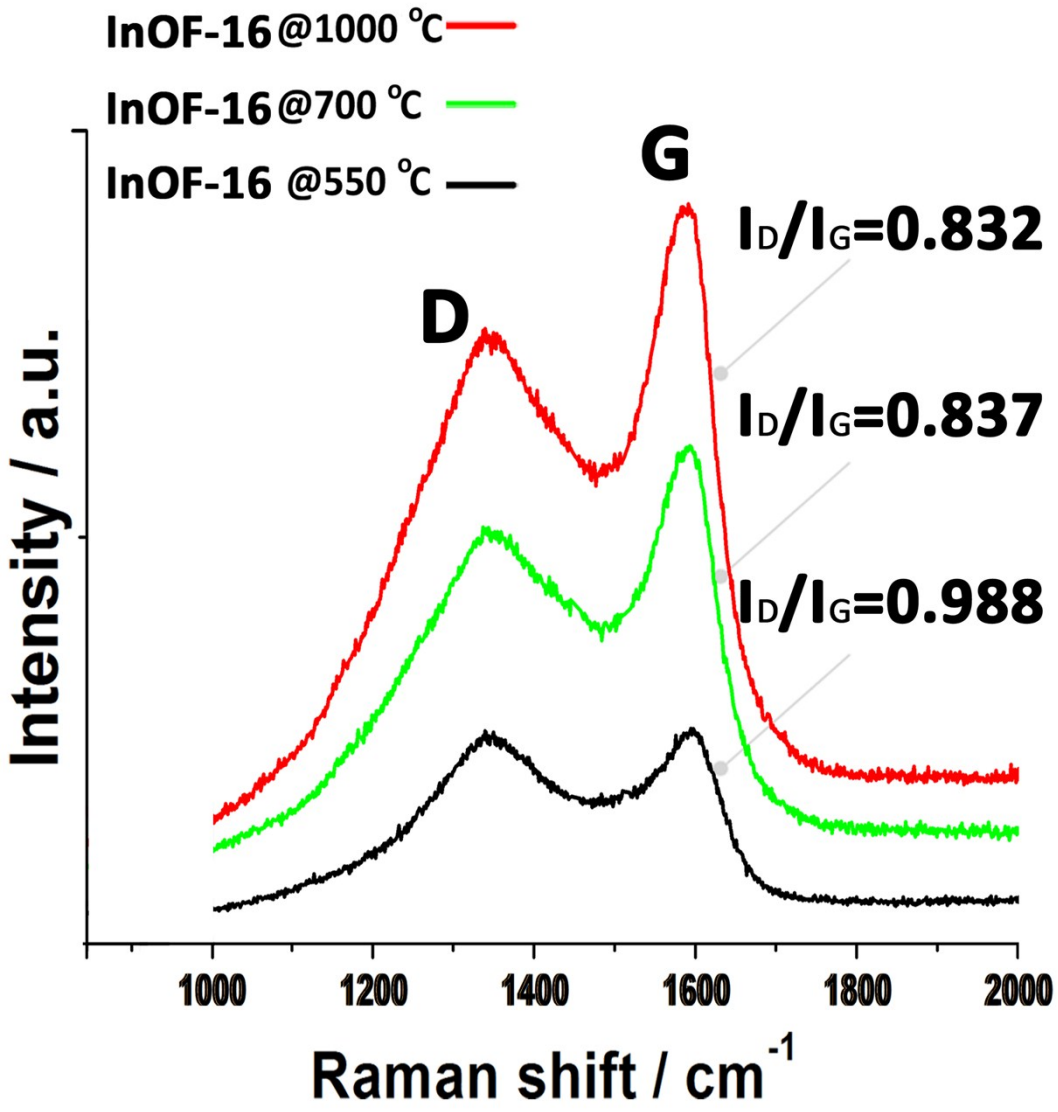

Figure S15. Raman spectra of **InOF-16-Ar-T** samples

We have learnt that carbon materials exist together with inorganic nanoparticles when heating in inert argon atmosphere, where a typical D band at approximately 1352 cm^{-1} results from the disordered sp^3-carbon, and a stronger G band (1589 cm^{-1}) from the crystalline graphitic carbon, and the intensity ratio of D/G bands (I_D/I_G) from 0.83-0.99 indicates that high carbonization temperature tends to expedite large degree of graphitization.

S11. XPS Survey Spectra

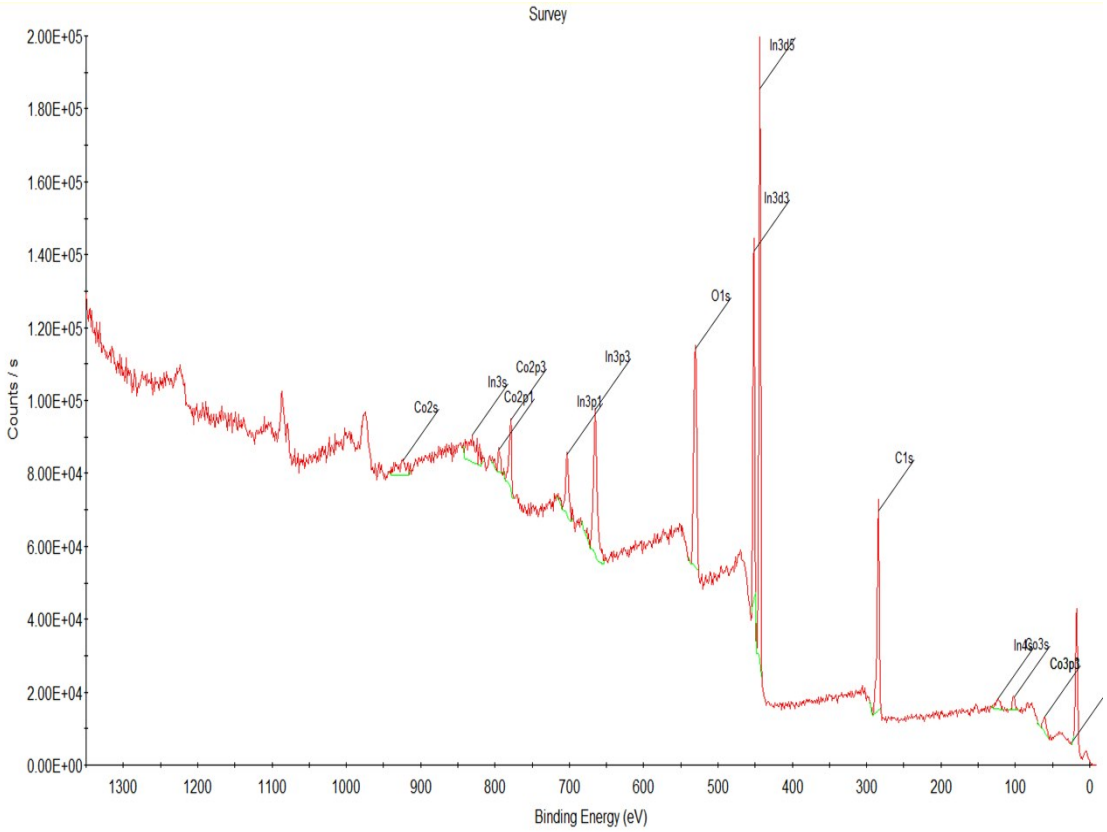

Figure S16. XPS survey spectra, the binding energies were obtained with reference to the C 1s at 284.6 eV for the as-prepared **InOF-16-O_2-1000** material.

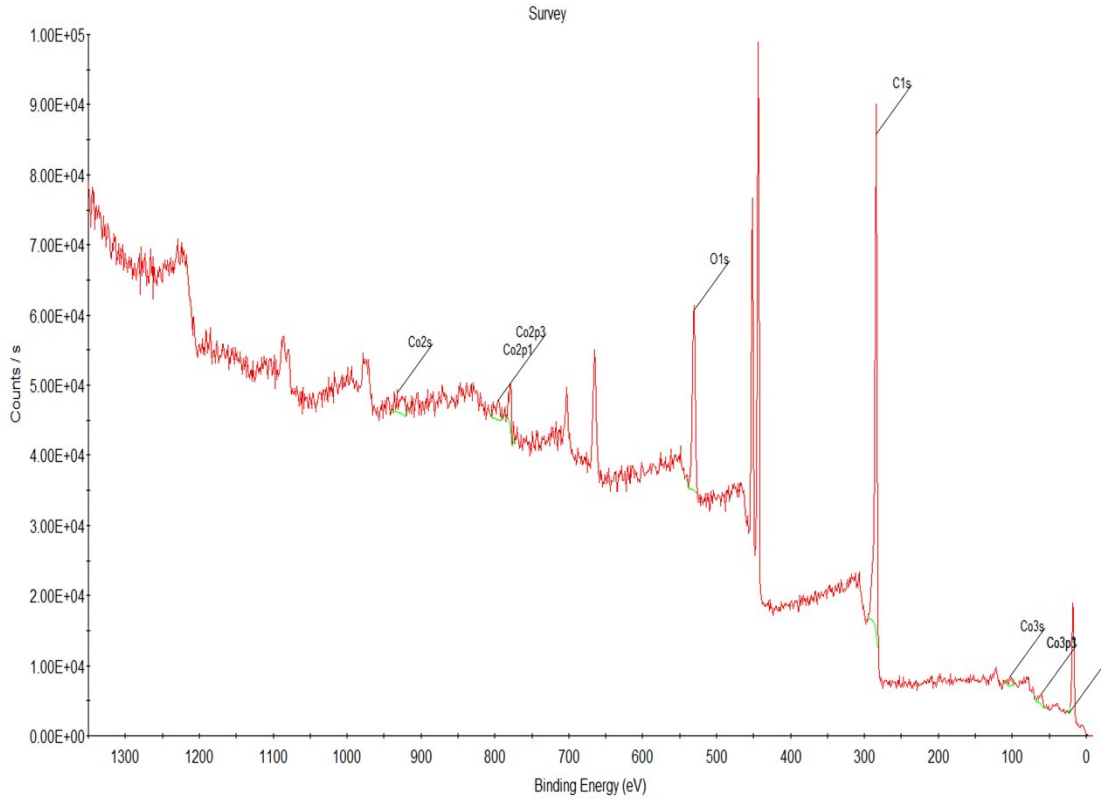

Figure S17. XPS survey spectra, the binding energies were obtained with reference to the C 1s at 284.6 eV for the as-prepared **InOF-16-Ar-1000** material.

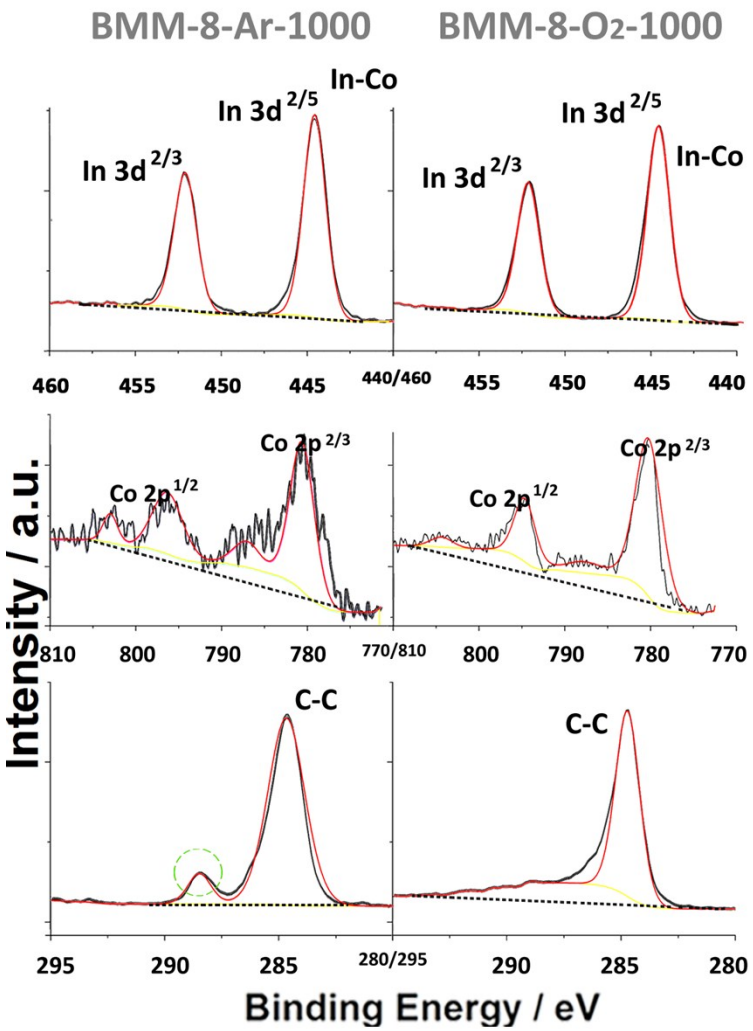

Figure S18. The deconvoluted In 3d, Co 2p and C 1s spectra of **InOF-16-Ar-1000** (Left) and **InOF-16-O_2-1000** (Right)

The states of Co, In and C atoms in the surface of both materials are analyzed by their deconvoluted XPS spectra (Figure S14). The peaks centred at 444.5, 780.2 and 284.6 eV for In $3d^{2/5}$, Co $2p^{2/3}$ and C1s signals could be attributed to Co-bonded indium atoms (In-Co), carbon-bonded cobalt (Co-C) and Co-bonded carbon atoms (C-Co) in both materials, respectively. Sparkly, there is a moderate oxygenated carbon atoms only in the external layers of **InOF-16-Ar-1000** material, corresponding to the peaks at 288.4 eV (C-O and/or C=O) in the corresponding C1s spectra. These oxygen ingredients can be observed only in **InOF-16-Ar-T** sample, indicating that it is derived from the preservation of carbon species in above-mentioned NPs@carbon-layer composite.

S12. Energy Dispersive Spectroscopy

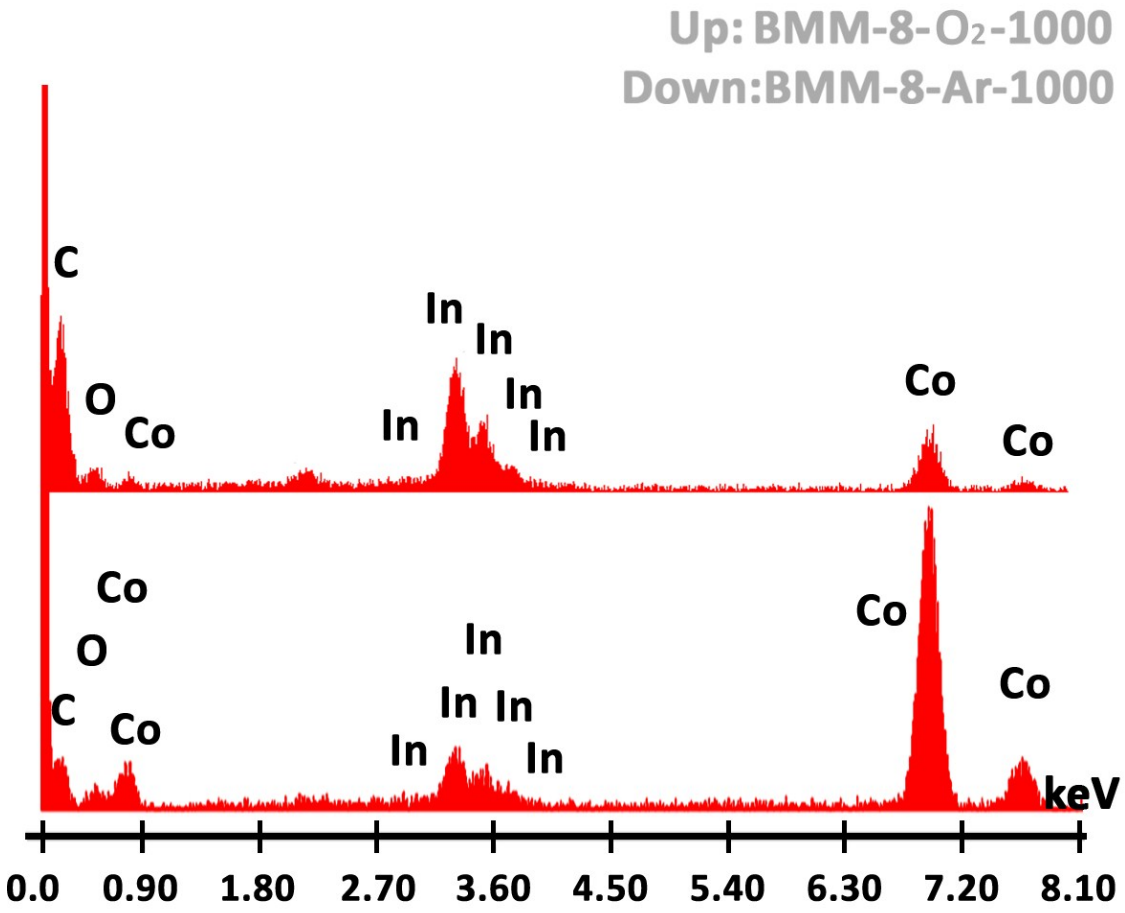

Figure S19. EDS figures for these two kinds of as-prepared **InOF-16** with different thermal treatment at 1000 °C. The energy dispersive spectroscopy exhibits that both samples consist of indium, cobalt and carbon elements.

S13. Electrochemical Measurements

Electrochemical method.

The working electrode was prepared via a drop-casting approach with the assistance of Nafion binders. Briefly, 6 mg MOF-derived powders was dispersed in 1.0 mL mixture of isopropanol and 5 wt% Nafion solution (9:1 v/v), the mixed solution was then sonicated for at least 30 min to form homogeneous inks, and finally 50 μL of the above inks was drop-casted onto the carbon cloth (0.5 cm^2) to obtain working electrode. All electrochemical measurements were conducted on a Shanghai Chenhua CHI660E electrochemical potentiostat rxwith a three-electrode setup. A Pt slice and an Ag/AgCl electrode (saturated KCl solution) were used as counter electrode and reference electrode, respectively. In the 1.0 M NaOH aqueous solution, the measured potentials were all converted to RHE scale via the equation: E vs.RHE = E vs.Ag/AgCl + 0.0592 × pH + 0.197. Prior to each electrochemical measurement, the electrolyte was degassed by bubbling with high purity nitrogen for 0.5 hour. Linear sweep voltammetry (LSVs) was measured at a scan rate of 5 mV s^{-1}. Electrochemical impedance spectroscopy (EIS) measurement was carried out at 1.60 V vs.RHE from 10^{-2} to 10^5 Hz with an AC amplitude of 5 mV. To evaluate the active surface area of catalysts, the double-layer capacitance (C_{dl}) was estimated by measuring the cyclic voltammetry at non-Faradaic region of 1.10 ~ 1.20 V vs.RHE under various scan rates from 10 to 50 mV s^{-1}. By plotting the current density at 1.15 V vs. RHE against the scan rate, a linear trend was observed, and the linear slope equivalent to C_{dl}.

And just like the procedure we used in the article, we have prepared working electrode was prepared via a drop-casting approach with the assistance of Nafion binders. Briefly, 6 mg MOF-derived powders was dispersed in 1.0 mL mixture of isopropanol and 5 wt% Nafion solution (9:1 v/v), the mixed solution was then sonicated for at least 30 min to form homogeneous inks, and finally 50 μL of the above inks was drop-casted onto the carbon cloth (0.5 cm^2) to obtain working electrode. Consequently, the linear sweep voltammetric measurements were also conducted for these two kinds of oxides for better comparisons.

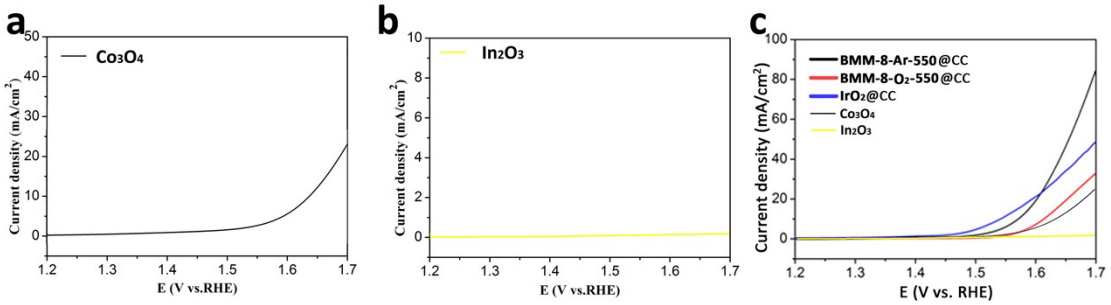

Figure S20. The CVs obtained in a 0.1 M KOH solution by using **FJI-6** derived Co_3O_4, **InOF-9** derived In_2O_3, and all materials in electrodes in our work.

As comparison in Figure S20, we learn that the **FJI-6** derived Co_3O_4 sample exhibits a moderate OER performance with 6.7 mA/cm^2 is achieved for Co_3O_4@Cc at 1.61 V, while the indium oxide from **InOF-9** is inactive with barely no current density being in the normal range of 1.2~1.7 (vs RHE). Finally, different electrodes with all the materials vary in the OER performance, and our **InOF-16-Ar-550**@CC is the best OER catalyst in this work.

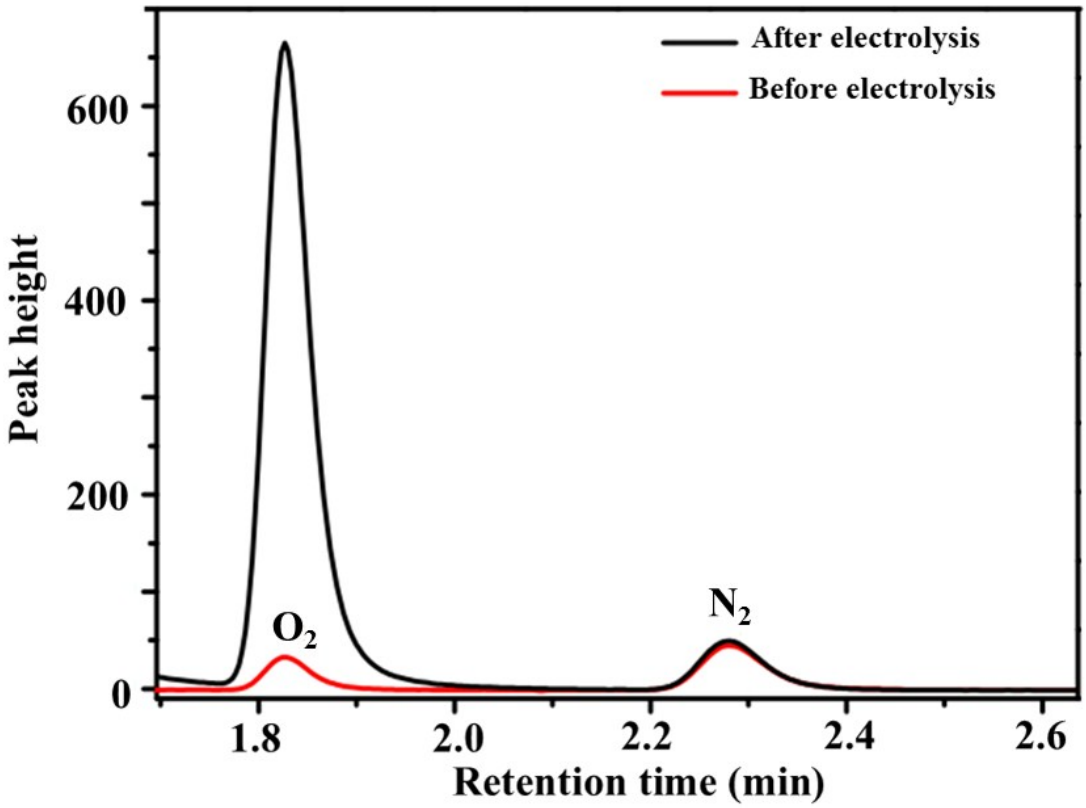

Figure S21. The amount of evolved oxygen was quantified by gas cinematographer (GC) method.

The amount of generated oxygen during CPE measurement was quantified by gas chromatography (GC) method through manual sampling with a gastight syringe, the calculated amount of O_2 was determined by dividing the recorded total passed charge by 4F.

$$\textbf{Faradaic efficiency (FE)} = n_{meas.O2}/n_{calcd.O2} \times 100\ \%.$$

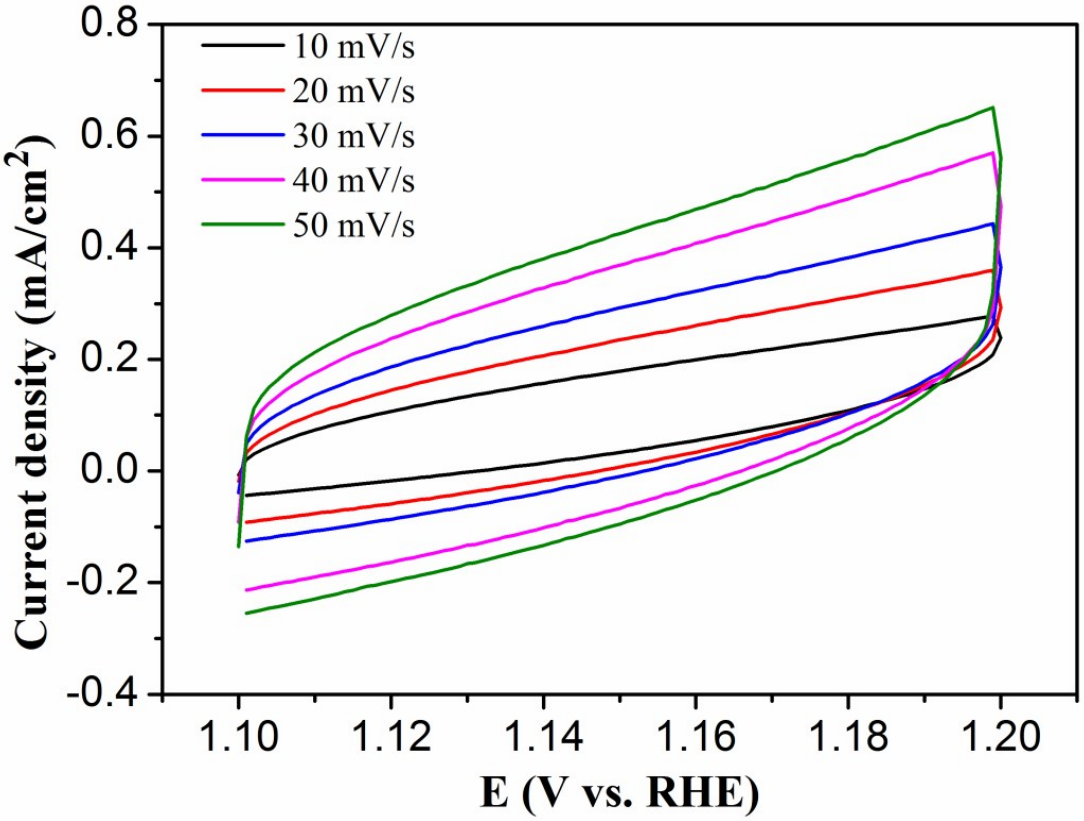

Figure S22. CV curves of **InOF-16-O_2-1000@CC** under various scan rates from 10 to 50 mV s^{-1} in the non-Faradaic potential range (1.10 – 1.20 V vs. RHE).

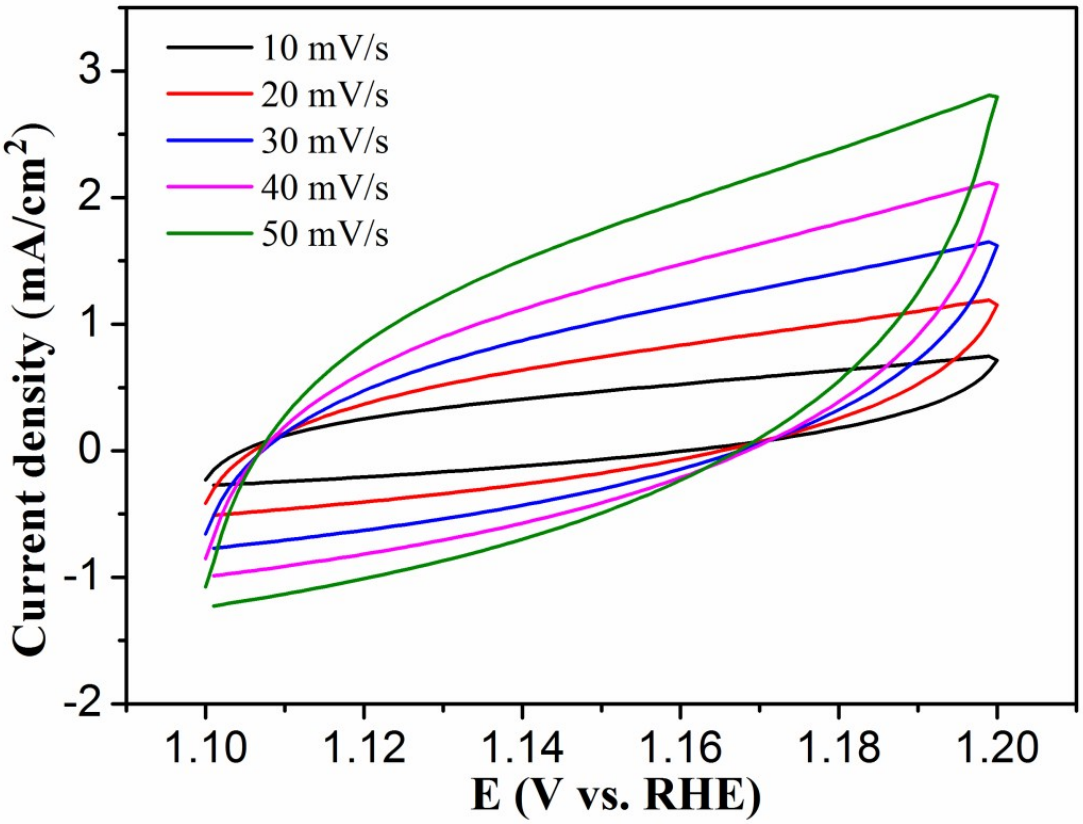

Figure S23. CV curves of **InOF-16-Ar-1000@CC** under various scan rates from 10 to 50 mV s^{-1} in the non-Faradaic potential range (1.10 – 1.20 V vs. RHE).

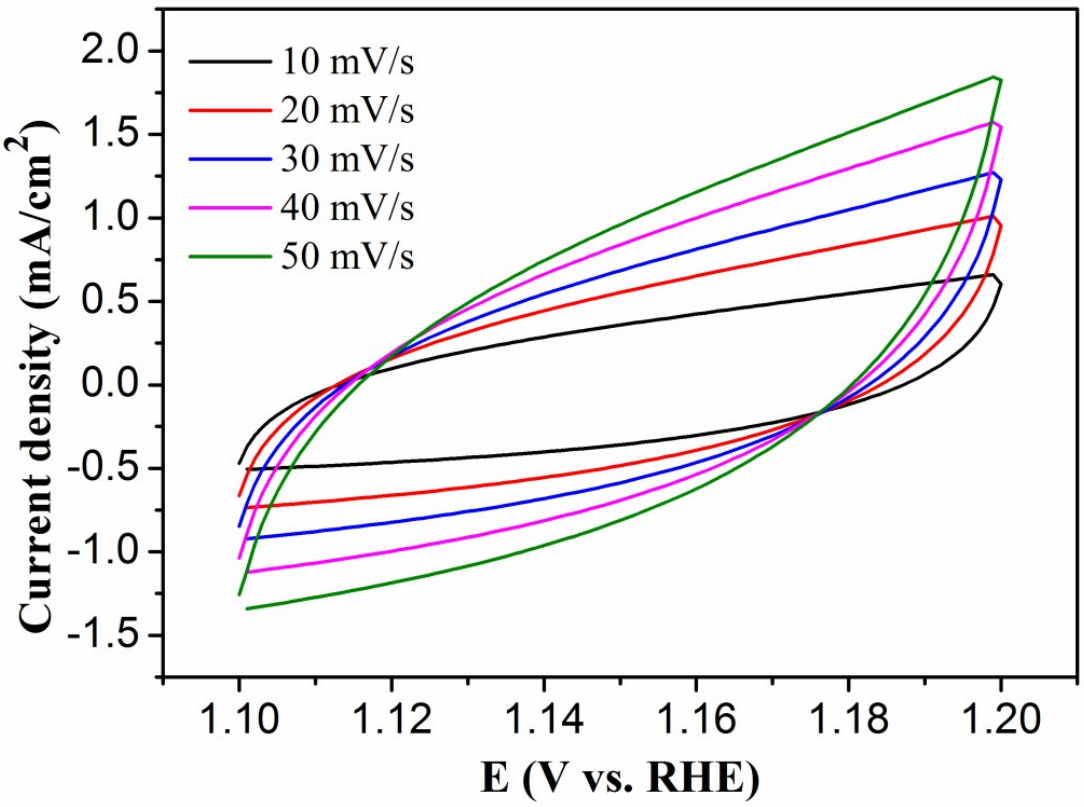

Figure S24. CV curves of IrO_2 under various scan rates from 10 to 50 mV s^{-1} in the non-Faradaic potential range (1.10 – 1.20 V vs. RHE).

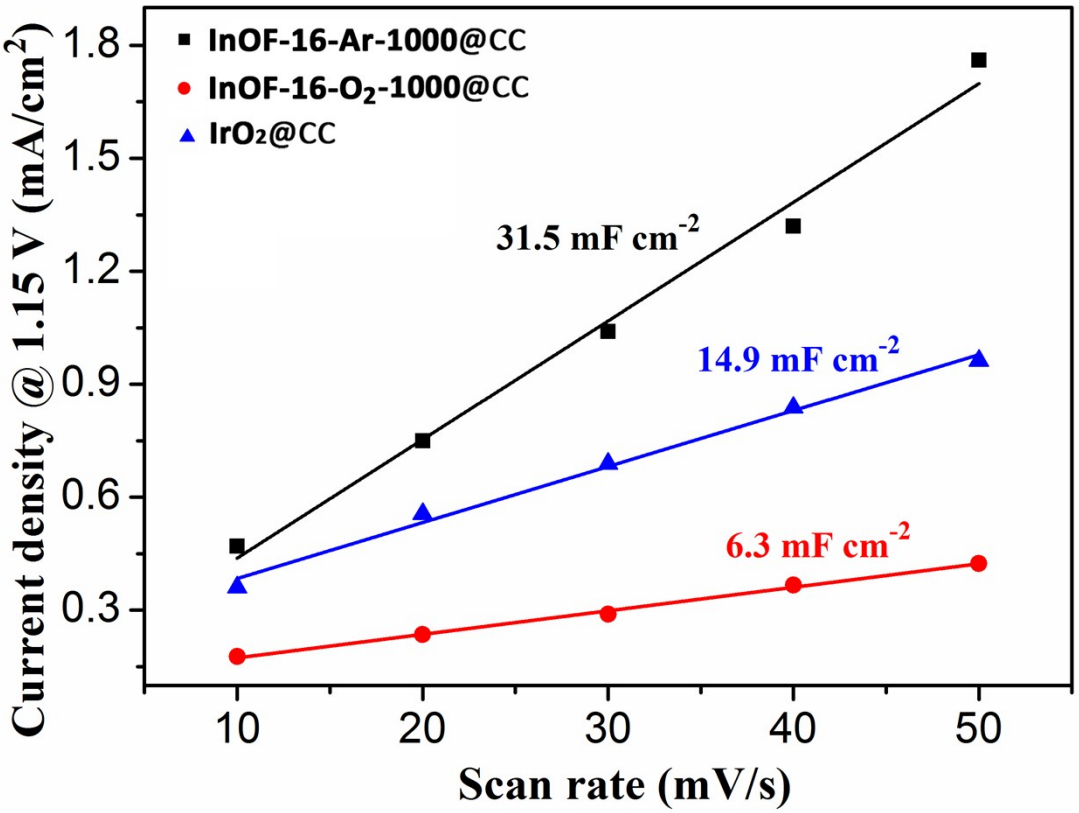

Figure S25. Plots of the current densities at 1.15 V vs. RHE against the scan rates.

The porous structures of **E1** afford effective active surface area, which is important on the surfaces of the catalysts. The active surface area can be reflected by the electrochemical double-layer capacitance (C_{dl}), the C_{dl} of **E1-3** were measured by recording the cyclic voltammograms of each material at different scan rates in the non-faradaic potential range, and the slope of capacitive current j vs. scan rate represents the C_{dl} value (Figure S18-S20). Accordingly, the C_{dl} of **E1** is fitted to be 31.5 mF cm^{-2}, which is almost 5-fold and 2-fold bigger than those of **E2** (6.3 mF cm^{-2}) and IrO_2 (14.9 mF cm^{-2}), indicating the larger electroactive surface area. Additionally, the enhanced exposure of active sites would facilitate the absorption and reaction of hydroxide anions with **E1** (Figure S25).

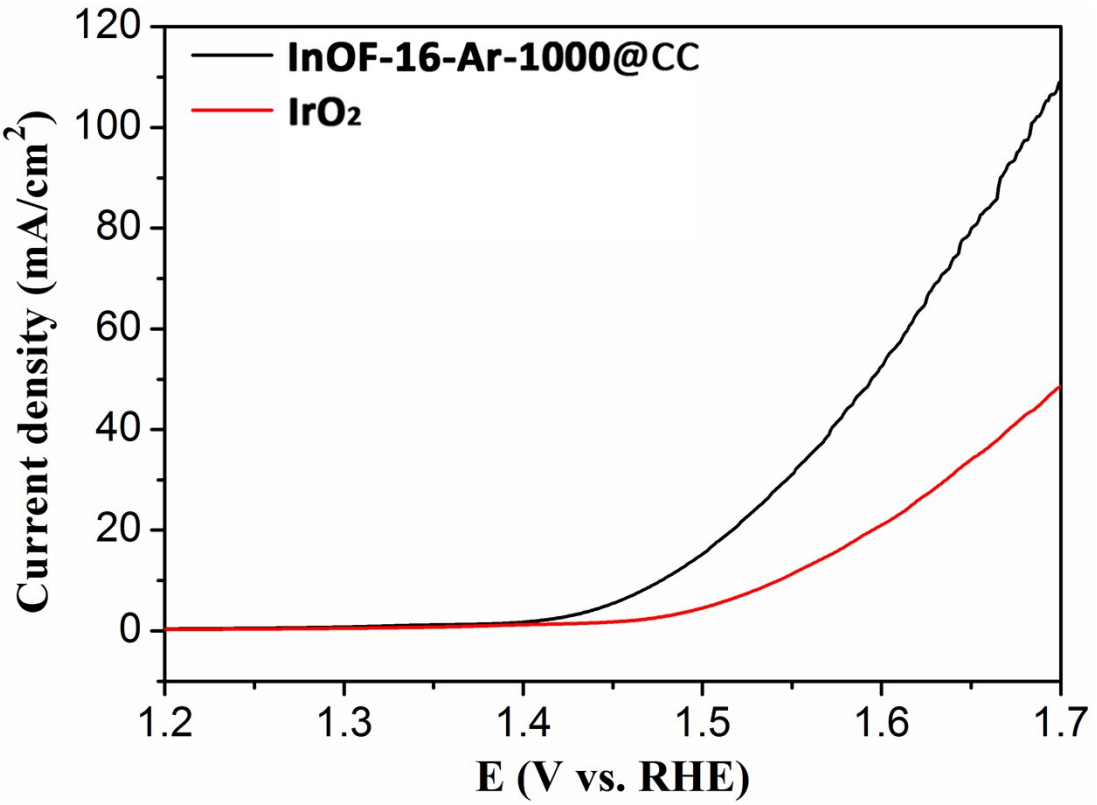

Figure S26. LSV plots of **InOF-16-Ar-1000@CC** and IrO_2**@CC** in 1.0 M NaOH at a scan rate of 5 mV s^{-1}

The LSV plots of these three samples are shown above in the main text, and the catalytic activities clearly enhanced with the increasing calcination temperature, the catalyst synthesized at 1000 ^{o}C presents the best OER activities, to achieve a 10 mA cm^{-2}, which is a metric related to solar fuel synthesis, **InOF-16-Ar-1000**, **InOF-16-Ar-700**, **InOF-16-Ar-550** and IrO_2 require overpotential of ~250, ~280, 370 and 350 mV, respectively.

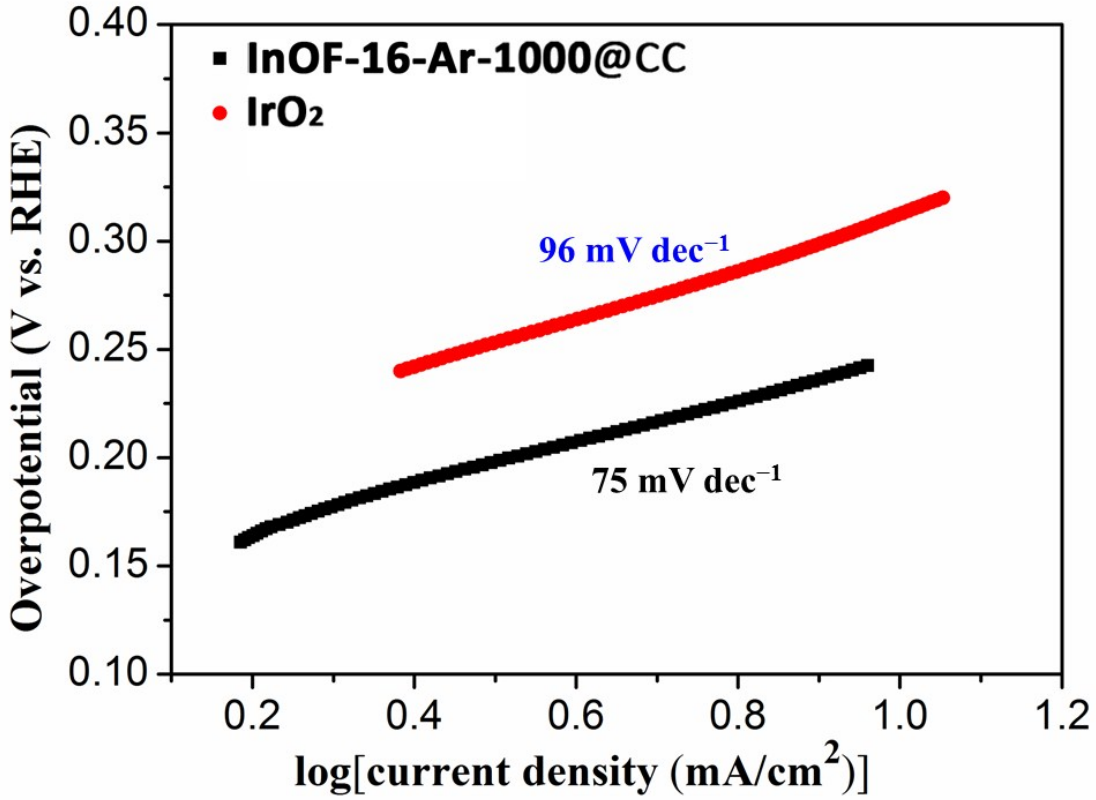

Figure S27. The Tafel plots of **InOF-16-Ar-1000@CC** and IrO_2@CC electrodes recorded in 1.0 M NaOH solution, the Tafel slope is derived from the polarization curves at a scan rate of 0.5 mV s^{-1}.

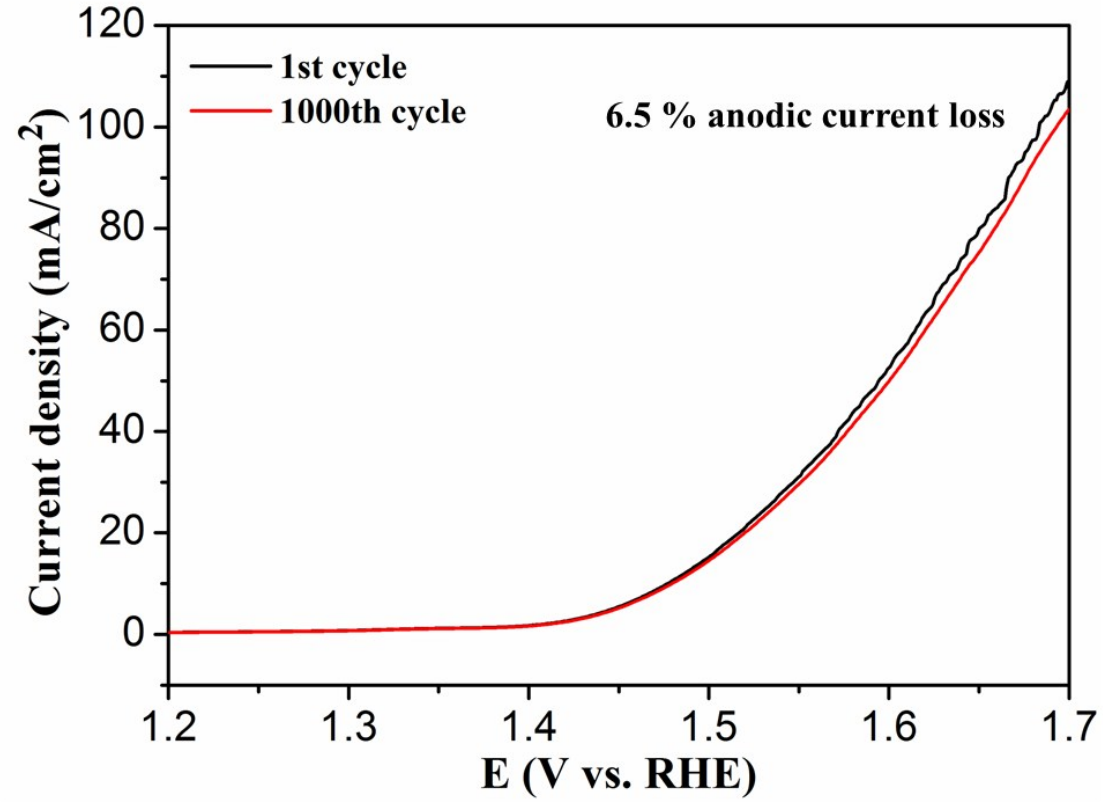

Figure S28. Durability test for **InOF-16-Ar-1000@CC** by LSV scan at 1000th cycles in 1.0 M NaOH solution.

Long-term stability of electrocatalyst is of great important for energy conversion practicability. First, the stability of **InOF-16-Ar-1000** was investigated by LSV cycling tests, after the 1000th cycle, 6.5 % loss of anodic current density compared with the initial cycle was observed

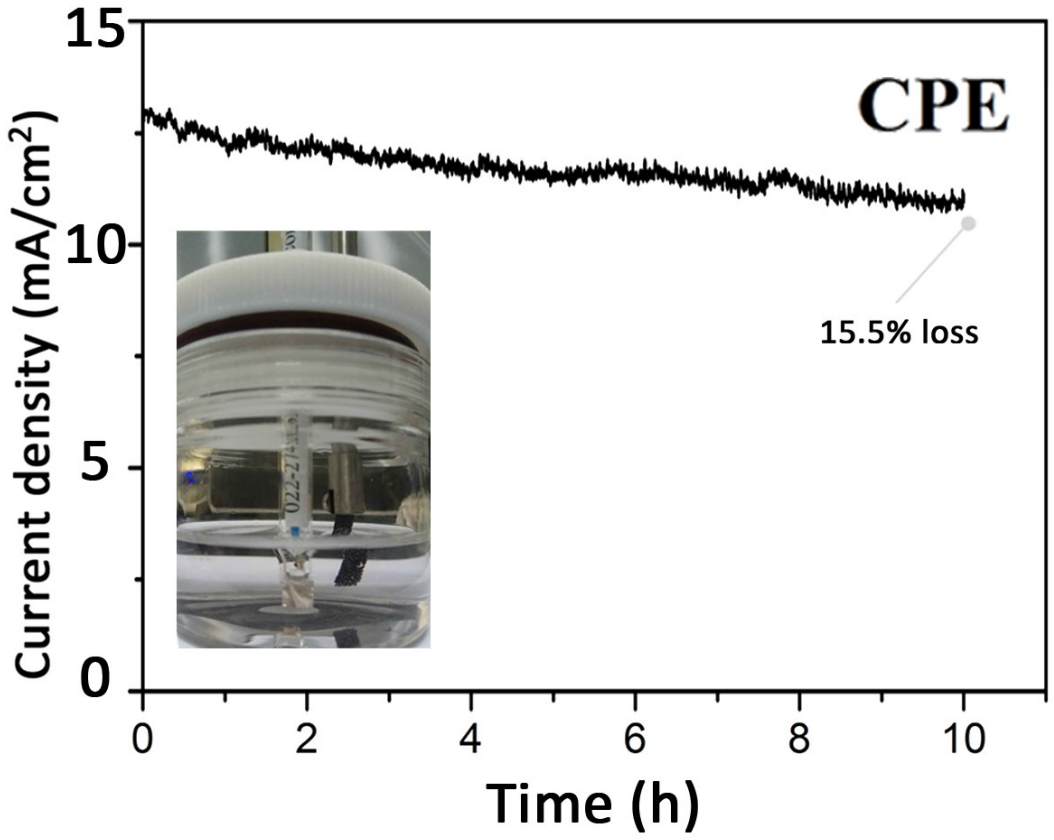

Figure S29. CPE measurement of **INOF-16-Ar-1000** at 1.55 V vs. RHE.

The **InOF-16-Ar-1000** was subjected to controlled potential electrolysis measurements at 1.55 V vs. RHE, a current density of 12.5 mA cm^{-2} was obtained at 84.5 % of its initial value over an electrolysis period of 10 hours.

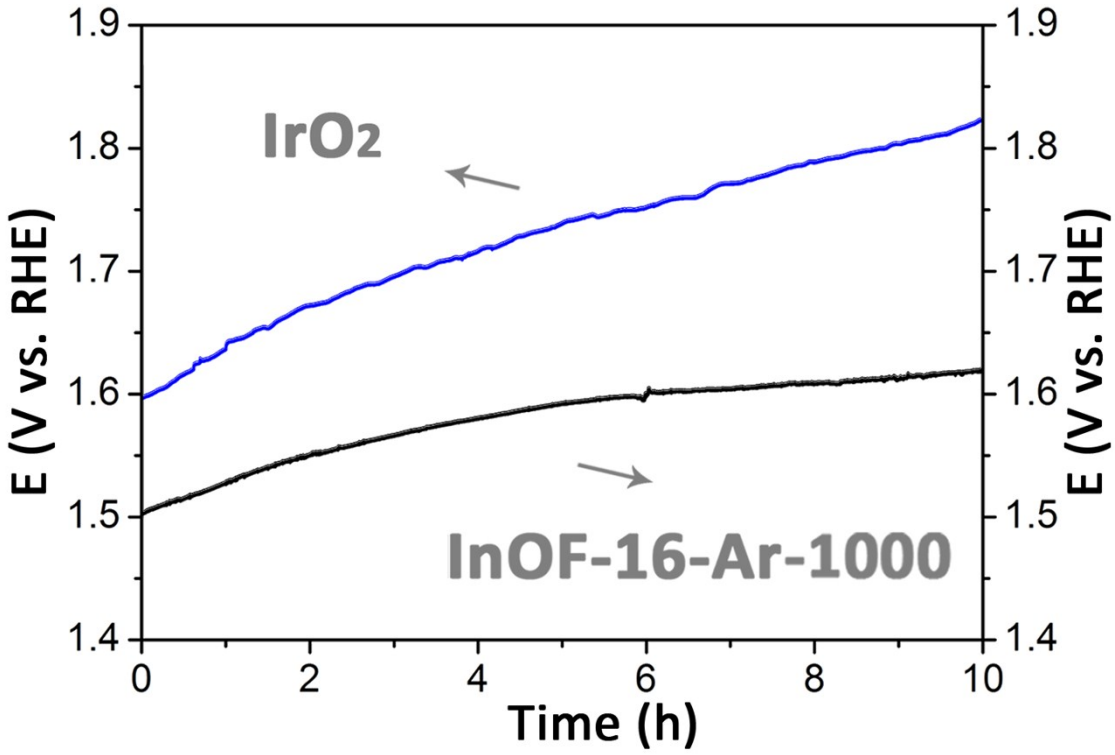

Figure S30. Chronopotentio-metric curves of **InOF-16-Ar-1000** (black) and IrO_2 (blue).

Besides, the chronopotentiometric responses demonstrate that it has much smaller OER activity attenuation when compared with that of IrO_2. For **InOF-16-Ar-1000**, only 8% potential increase at a constant current density of 10 mA cm^{-2} after 10 h, whereas IrO_2 requires a 2-fold increase in potential under the same condition.

Table S5. Comparisons of OER activities of some recently reported Co-MOFs derived catalysts.

Catalyst	MOF	E_{onset} (V vs.RHE)[a]	$E_j = 10$ (V vs.RHE)[b]	Tafel plot (mV dec^{-1})	Mass loading (mg cm^{-2})	Electrolyte	Support	Reference
InOF-16-Ar-1000	**InOF-16**	1.45	1.48 V	75	0.60	1.0 M NaOH	CC[c]	**This work**
Porous Co_3O_4	**ZIF-67**	1.58	1.69	89	0.35	0.1 M KOH	GCE[d]	**S5**
Co/MIL-101 (Cr)-O	**MIL-101 (Cr)**	N.A.	1.72	122	0.24	0.1 M KOH	GCE	**S6**
Co_3O_4/N-PC	**ZIF-67**	1.52	1.62	72	0.35	0.1 M KOH	GCE	**S7.**
Co_3O_4@C-MWCNTs	**ZIF-9**	1.50	1.82	N.A.	0.13	0.1 M KOH	GCE	**S8**
$Co_3O_4/NiCo_2O_4$ DSNCs	**ZIF-67**	1.53	1.57	88	1.0	1.0 M KOH	NF[e]	**S9**
Co_3O_4C-NA	**Co-MOF**	1.41	1.45	61	~0.20	1.0 M KOH	Cu foil	**S10**
$CoFe_2O_4$/C NRAs	**MOF-74**	1.45	1.47	45	1.03	1.0 M KOH	NF@NC[f]	**S11**
Co_3O_4/C NA	**Co-MOF**	1.52	N.A.	81	1.70	1.0 M KOH	Ni foam	**S12**
UTSA-16	**UTSA-16**	1.60	1.64	77	0.35	1.0 M KOH	GCE	**S13**
Co–CNT/PC	**ZIF-67**	1.49	1.55	73.8	1	0.1 M KOH	Ni foam	**S14**

a: E_{onset} for onset potential for water oxidation; b: $E_j = 10$ for the potential required for the current density of 10 mA cm^{-2}; c: CC for carbon cloth; d: GCE for glassy carbon electrode; e: NF for Nickel foam; f: NF@NC for nitrogen doped carbon on Nickel foam.

It should be pointed out that the overpotential of **InOF-16-Ar-1000** to deliver a 10 mA cm^{-2} current density is lower than those of most non-precious hybrid OER electrocatalysts, and also compares favorably to those of MOF-derived nanowire array anodes (please see the detail in Table S5, Supporting Information). In addition, the **InOF-16-Ar-1000** was subjected to controlled potential electrolysis measurements at 1.55 V vs. RHE, a current density of 12.5 mA cm^{-2} was obtained at 84.5 % of its initial value over an electrolysis period of 10 h (Fig. S29). The amount of evolved oxygen was quantified by gas chromatographer (GC) method and the Faradaic efficiency of **InOF-16-Ar-1000** for OER was measured to be 98.5 %.

Long-term stability of electrocatalyst is of great important for energy conversion practicability. First, the stability of **InOF-16-Ar-1000** was investigated by LSV cycling tests, after the 1000th cycle, only 6.5 % loss of anodic current density compared with the initial cycle was observed (Fig. S28). Besides, the chronopotentiometric responses demonstrate that it has much smaller OER activity attenuation when compared with that of IrO_2. For **InOF-16-Ar-1000**, only 8% potential increase at a constant current density of 10 mA cm^{-2} after 10 h (Fig. S30), whereas IrO_2 requires a 2-fold increase in potential under the same condition. Based on the above results, the catalytic activity and durability of **InOF-16-Ar-1000** is superior to that of the state-of-the-art IrO_2 catalyst.

S14. Reference

[S1] *J. Appl. Cryst*. **2009**, *42*, 339.

[S2] *Acta Cryst*. **2008**, *A64*, 112.

[S3] *Acta Cryst*. **2008**, *A64*, 112.

[S4] a) S. T. Zheng, J. T. Bu, Y. F. Li, T. Wu, F. Zuo, P. Y. Feng, X. H. Bu, *J. Am. Chem. Soc.* **2010**, *132*, 17062-17064; b) J. J. Qian, F. L. Jiang, D. Q. Yuan, X. J. Li, L. J. Zhang, K. Z. Su, M. C. Hong, *J. Mater. Chem. A.* **2013**, *1*, 9075-9082.

[S5] *J. Power Sources*. **2015**, *294*, 103

[S6] *Int. J. Hydrogen Energy*. **2015**, *40*, 9713.

[S7] *Nano Energy*. **2015**, *12*, 1.

[S8] *J. Mater. Chem*. A. **2015**, *3*, 17392

[S9] *J. Am. Chem. Soc*. **2015**, *137*, 5590.

[S10] *J. Am. Chem. Soc*. **2014**, *136*, 13925.

[S11] *Adv. Mater*. **2016**, DOI: 10.1002/adma.201604437

[S12] *J. Mater. Chem. A*. **2016**, *4*, 16516.

[S13] *ACS Appl. Mater. Interfaces,* **2017**, *9*, 7193.

[S14] *Chem. Commun.*, **2016**, *52*, 9727.